Current Research in Pharmacology and Drug Discovery 2 (2021) 100038

Contents lists available at ScienceDirect

Current Research in Pharmacology and Drug Discovery

journal homepage: www.journals.elsevier.com/current-research-in-pharmacology-and-drug-discovery

Potential inhibitors of SARS-CoV-2 (COVID 19) proteases PL^{pro} and M^{pro}/$3CL^{pro}$: molecular docking and simulation studies of three pertinent medicinal plant natural components

Devvret Verma [a,1,*], Debasis Mitra [b,1], Manish Paul [c,1], Priya Chaudhary [d], Anshul Kamboj [a], Hrudayanath Thatoi [c], Pracheta Janmeda [d], Divya Jain [d], Periyasamy Panneerselvam [e], Rakesh Shrivastav [f], Kumud Pant [a], Pradeep K. Das Mohapatra [b,g,**]

[a] Department of Biotechnology, Graphic Era (Deemed to be University), Dehradun, 248 002, Uttarakhand, India
[b] Department of Microbiology, Raiganj University, Raiganj, 733 134, Uttar Dinajpur, West Bengal, India
[c] Department of Biotechnology, Maharaja Sriram Chandra Bhanja Deo University, Baripada, 757003, Odisha, India
[d] Department of Bioscience and Biotechnology, Banasthali University, Vanasthali, 304022, Rajasthan, India
[e] Microbiology, Crop Production Division, ICAR- National Rice Research Institute, Cuttack, 753 006, Odisha, India
[f] Department of Applied Sciences, NGF College of Engineering and Technology, Palwal, Haryana, India
[g] PAKB Environment Conservation Centre, Raiganj University, Raiganj, 733 134, Uttar Dinajpur, West Bengal, India

ARTICLE INFO

Keywords:
SARS-CoV-2 (COVID-19)
PL^{pro}-M^{pro}/$3CL^{pro}$
Canthin-6-one 9-O-Beta-glucopyranoside
Natural inhibitor
Molecular dynamics

ABSTRACT

The rapid spread of severe acute respiratory syndrome coronavirus 2 (SARS-CoV-2) - coronavirus disease 2019 (COVID-19) has raised a severe global public health issue and creates a pandemic situation. The present work aims to study the molecular -docking and dynamic of three pertinent medicinal plants *i.e. Eurycoma harmandiana*, *Sophora flavescens* and *Andrographis paniculata* phyto-compounds against SARS-COV-2 papain-like protease (PL^{pro}) and main protease (M^{pro})/3-chymotrypsin-like protease ($3CL^{pro}$). The interaction of protein targets and ligands was performed through AutoDock-Vina visualized using PyMOL and BIOVIA-Discovery Studio 2020. Molecular docking with canthin-6-one 9-O-beta-glucopyranoside showed highest binding affinity and less binding energy with both PL^{pro} and M^{pro}/$3CL^{pro}$ proteases and was subjected to molecular dynamic (MD) simulations for a period of 100ns. Stability of the protein-ligand complexes was evaluated by different analyses. The binding free energy calculated using MM-PBSA and the results showed that the molecule must have stable interactions with the protein binding site. ADMET analysis of the compounds suggested that it is having drug-like properties like high gastrointestinal (GI) absorption, no blood-brain barrier permeability and high lipophilicity. The outcome revealed that canthin-6-one 9-O-beta-glucopyranoside can be used as a potential natural drug against COVID-19 protease.

1. Introduction

The illness caused by severe acute respiratory syndrome coronavirus 2 (SARS-CoV-2) is named coronavirus disease 2019 (COVID-19) (Zhang et al., 2020a; Mohamed and Fatima, 2020; Chaudhary and Janmeda, 2020). By 24th April 2021, beyond one hundred forty-four million sufferers were documented globally, with greater than three million sixty-six thousands of demises (223 countries, areas or territories with cases) which resume to rising, majorly in India, USA, Western Pacific, South-east Asia, Europe, Africa, and Eastern Mediterranean, as these are nations with a huge fragment of elderly inhabitants who have been infected with the SARS-CoV-2 (WHO, 2020; https://www.who.int/emergencies/diseases/novel-coronavirus-2019). SARS-CoV-2 is a non-segmented, enveloped, and positive-sense RNA virus. Structurally, SARS-CoV-2 comprises of four structural proteins including nucleocapsid protein (N), membrane glycol protein (M), small envelope glycoprotein (E), and spike protein (S). S protein generates homotrimers which are protruding on the surface of the virus and facilitate its binding to host cells by attracting angiotensin-converting enzyme 2 presented in lower respiratory tract cells. N protein is involved in the interaction with the viral genome and M protein and in virion assembly. M protein determines

* Corresponding author. Department of Biotechnology, Graphic Era (Deemed to be University), Dehradun, 248 002, Uttarakhand, India.
** Corresponding author. Department of Microbiology and PAKB Environment Conservation Centre, Raiganj University, Raiganj, 733 134, Uttar Dinajpur, West Bengal, India.
E-mail addresses: devvret@gmail.com (D. Verma), pkdmvu@gmail.com (P.K. Das Mohapatra).
[1] These authors have contributed equally to this work.

https://doi.org/10.1016/j.crphar.2021.100038
Received 26 April 2021; Received in revised form 28 May 2021; Accepted 1 June 2021

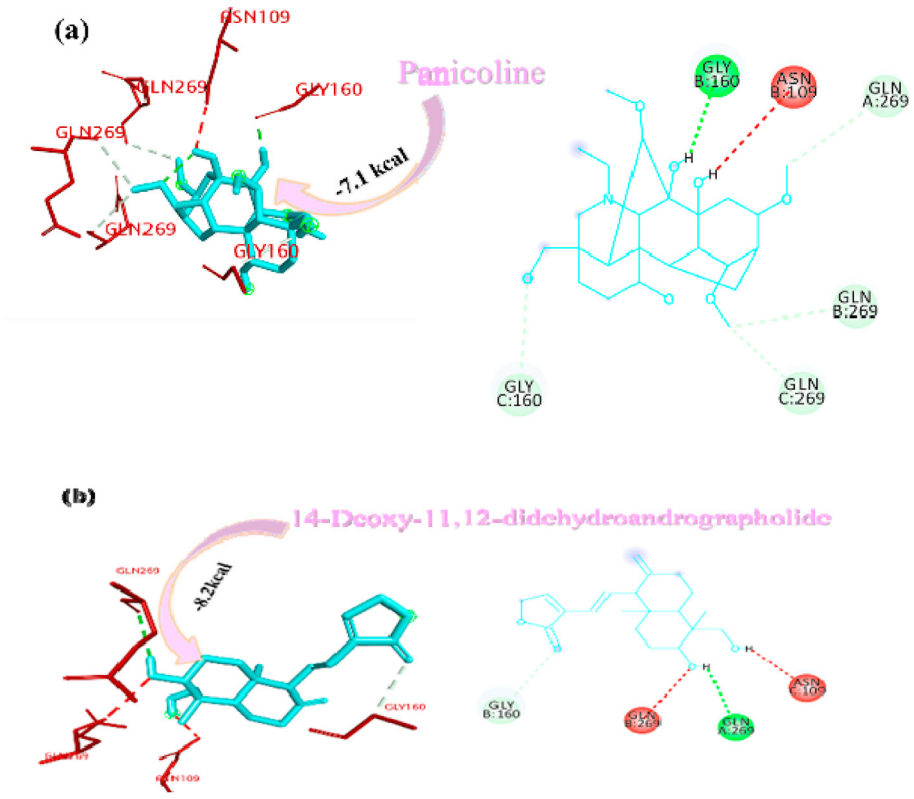

Fig. 1. Interactions established after docking the secondary metabolite against SARS-CoV-2 PL^{pro} Protein (6W9C). The interacting residues of the protein are labeled in purple and the docking scores are listed under each of the complex, respectively. The receptor-ligand interaction is represented on a 3D diagram (Right) and 2D diagram (Left). Drugs are in cyan and interacting atoms of protein are represented red in the diagram, while green dotted lines represent the conventional h-bond interactions, light green dotted line represents weak van der Waals interactions. Additionally, dotted lines in sky blue display the pi-donor hydrogen bond, pi-sigma interaction is shown as violet dashed lines, pink dotted lines show alkyl and pi-alkyl interactions, respectively.

the shape of the viral envelope. Basically, it stabilizes the N protein and allows the completion of viral assembly by stabilizing the N protein-RNA complex. The last structural protein is E protein which plays an important role in the maturation and production of the virus (Astuti and Ysrafil, 2020). After successful fusion and entry, the viral genome is released and ORF1a and ORF1b of genomic RNA are translated in two kinds of big polyproteins (pp1a and pp1 ab) that are cleaved in several functional viral proteins by viral proteases, main protease or 3-chymotrypsin-like protease (M^{pro}/$3CL^{pro}$) and papain-like proteases (PL^{pro}) that are encoded in nsp5 and nsp 3. (Mitra et al., 2021; de Oliveira et al., 2020; Khan et al., 2020). pp1a and pp1ab are cleaved in into nonstructural proteins (1–11 and 1–10, and 12–16) which play an important role in various processes during the virus life cycle (V'Kovski et al., 2020). M^{pro} is recognized for its significant role in enzymatic activity which leads to post-translational processing of replicase protein. It consists of 306 amino acids and shows a great resemblance with SARS-CoV-2 M^{pro}. It also comprises of three domains (C-terminal domain-III, N-terminal domain-II, and N-terminal domain-I) and two catalytic dyads (H41 and C145) (Amin et al., 2021). PL^{pro} is one of the main components of the SARS-CoV-2 replicase-transcriptase complex and its topological structure is divided into ubiquitin-like fingers, palm, and thumb. Basically, it carries out the processing of viral protein by identifying the Leu-X-Gly-Gly tertrapeptide motif and functions as de-ISGylating and de-ubiquitinating enzyme that inhibits the inflammatory signaling in the host cell (Li et al., 2021). Because of the pivotal roles and crucial function, the proteases perform in the life-cycle of the virus, they are a crucial target for the discovery of antiviral agents for SARS-CoV-2 (Arya et al., 2020; Kumar and Singh, 2020; Zhang et al., 2020b). At present, no drug has been invented, and hence because of the risk factors related to this illness, there is a critical requirement for a treatment (Enayatkhani et al., 2020). Currently, the idea of drug reuse is popularly utilized for the cure of variable disorders as it lessens the time, cost, and uncertainty of the drug generation operation by using a rapid computational perspective (Boopathi et al., 2019; Muralidharan et al., 2020).

Eurycoma harmandiana Pierre is a small plant, belongs to the Simaroubaceae family, allocated in the dividing line between Laos and Thailand (Kanchanapoom et al., 2001). Two alkaloids, 7-hydroxy-β-carboline 1-propionic acid and canthin-6-one 9-O-beta-glucopyranoside from the root part of *E. harmandiana* used as anti-viral agents (Kanchanapoom et al., 2001). Docking study of canthin-6-one 9-O-beta--glucopyranoside with NS1 protease to find out its effectiveness against the dengue virus, showed hydrogen bonds with the backbone and a side chain of SER^{80} and to THR^{87} and ASN^{130} side chains (ul Qamar et al., 2019). *Sophora flavescens* is a small Fabaceous plant, related to the Sophora genus. The roots of *S. flavescens* are termed as Kushen. It is broadly distributed in the regions of the Pacific Islands, Oceanica and the Asia, and has been greatly utilized as conventional herbal medication for the therapy of pain, scabies, myocarditis, cancer, dysentery, fever, and viral hepatitis (Kim et al., 2018). Many of the compounds were isolated from the roots of *S. flavescens* but out of them, kushenol W and kushenol K are utilized for carried the study of molecular docking in case of dengue virus. *Andrographis paniculata* (Burm. F) Nees, is an herbaceous plant, belongs to the Acanthaceae family. It has conventionally been utilized in China, Sri Lanka, India, and some other Southeast Asian countries. This plant is broadly acknowledged for its anti-inflammatory action against the infection of an upper respiratory tract (Mussard et al., 2019). Several compounds such as 3α, 14, 15, 18-Tetrahydroxy-5β, 9βH, 10α-labda-8, 12-dien-16-oic acid γ-lactone, deoxyandrographolide, neoandrographolide, 14-deoxy-11, 12-didehydroandrographolide, deoxyandrographolide19β-d-glucoside, 5,7,2′,3′-tetramethoxyflavanone, 5-Hydroxy-7,2′,3′-trimethoxyflavone, 14-Deoxy-11-oxoandrographolide, 5-Hydroxy-7,8,2′,3′-Tetramethoxyflavone, 5-Hydroxy-7,8,2′-Trimethoxyflavone, andrographine, panicoline, paniculide-A, paniculide-B, and paniculide-C have been reported from *A. paniculata*. According to

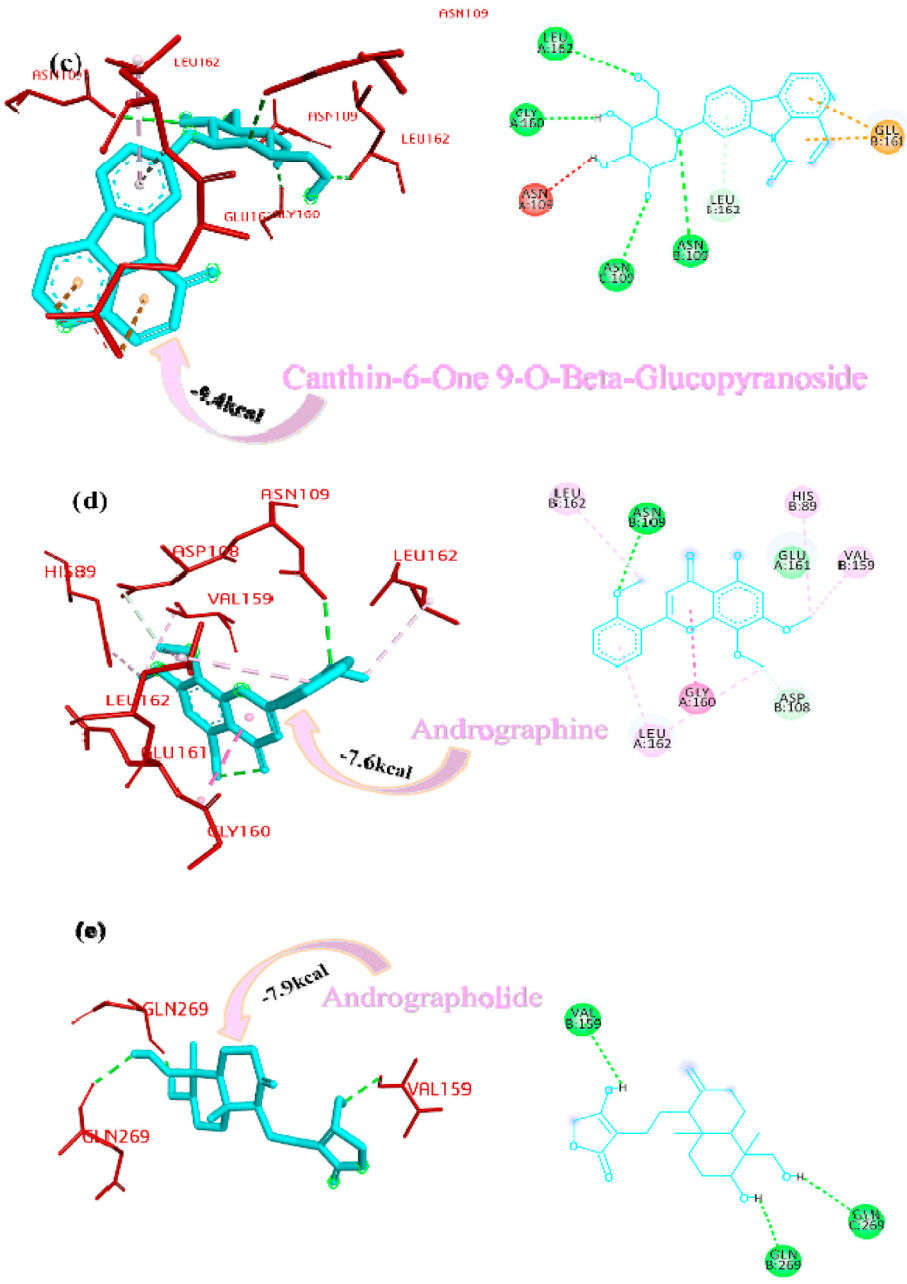

Fig. 1. (*continued*).

JayaKumar et al. (2013) many of the physicians have manufactured several derivatives of andrographolide, which manifests remarkable remedial activities such as antiviral, antifeedant, anti-HIV, antidiabetic, antitumor, antibacterial, and anti-inflammatory. The concentration and composition of chemical constituents in plants are greatly affected by variable factors like harvesting condition, growth condition, genetic factors, types of extraction solvent, and concentration of solvents (Rafi et al., 2020). So, the present investigation is concentrated on the identification of natural composite with an exclusive objective to speed up the recognition of particular medication for the treatment of SARS-CoV-2.

2. Materials and methods

2.1. Medicinal plant and their natural components

A. paniculata, *E. harmandiana* and *S. flavescens* are highly valuable medicinal plants as reported by many researchers (ul Qamar et al., 2019; Mussard et al., 2019; JayaKumar et al., 2013; Rafi et al., 2020). They are mainly used as an herbal remedy for the treatments of lung, sore throat, flu and upper respiratory tract infections, and possess inhibitors activity of NS1, NS3/NS2B and NS5 proteins of dengue virus and anti-inflammatory, anti-tumor, anti-HIV, antibacterial, antifeedant, antidiabetic, antiviral & other pharmacological activities. The molecular properties of the natural components of three pertinent medicinal plants were retrieved from the PubChem database (https://pubchem.ncbi.nlm.nih.gov/) as listed in Supplementary Table 1 (Kim et al., 2016).

2.2. Protein preparation

The crystal structure of papain-like protease (PL^{pro}), and 3-chymotrypsin-like protease ($3CL^{pro}$/M^{pro}) with PDB IDs 6W9C and 6M2N, respectively were retrieved from the Research Collaboratory for Structural Bioinformatics Protein Databank (RCSB PDB), https://www.rcsb.org/(Berman et al., 2000). All the crystal structures were prepared by removing existing ligands and water molecules by PyMOLv2.3.3, which is comprehensive molecular visualization software that enables users to

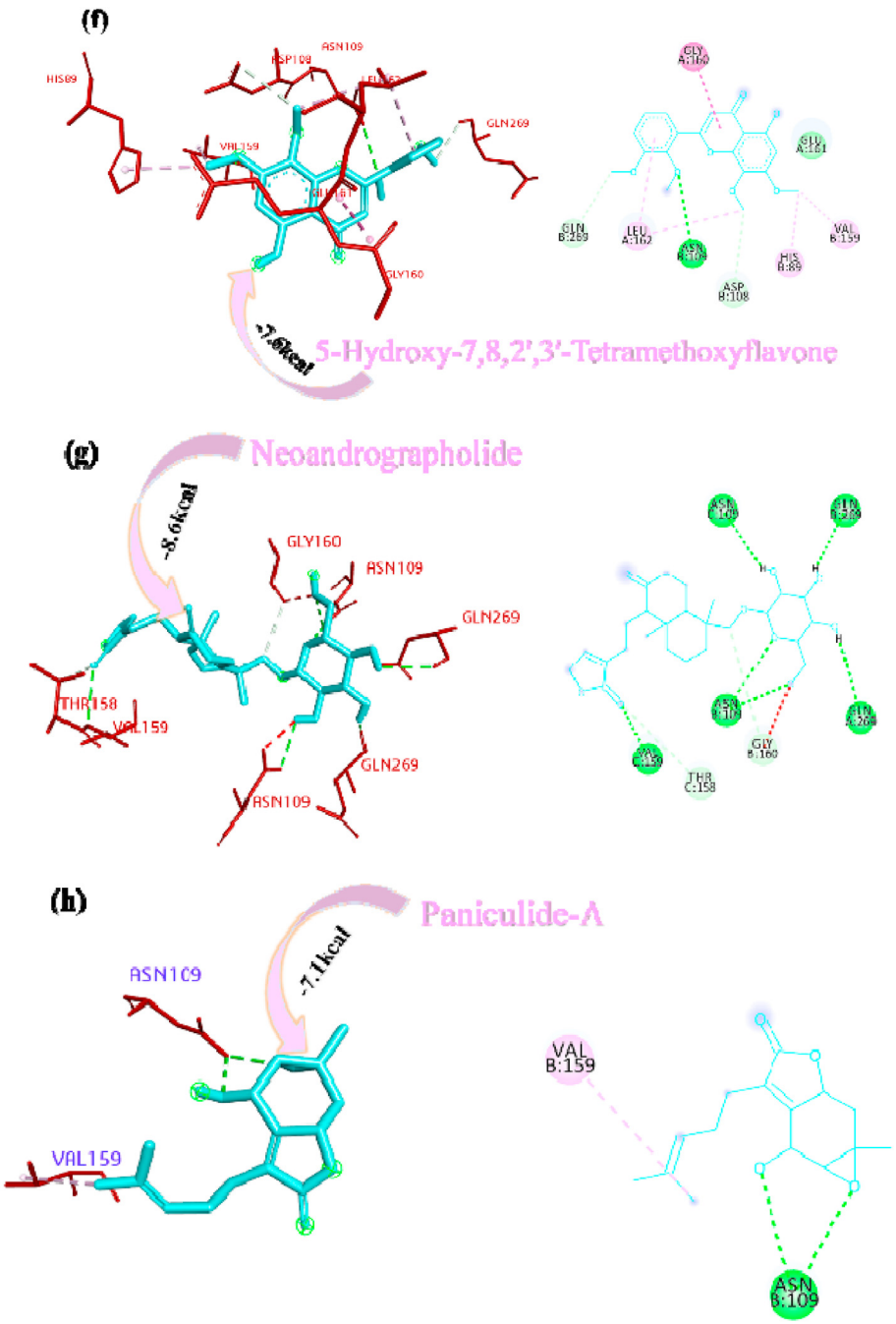

Fig. 1. (*continued*).

observe the three-dimensional (3D) structures of the compounds (PyMOL, 2020; https://pymol.org/2/).

2.3. Ligand preparation

The 3D structures of phytochemicals and drugs were retrieved from the PubChem database, www.pubchem.ncbi.nlm.nih.gov (Kim et al., 2016). The ligands were then further converted into the.pdbqt format using an open babel tool for molecular docking (Dallakyan and Olson, 2015).

2.4. Protein-molecular docking and building complexes

Molecular docking approaches are the best techniques for forecasting the reactions between drugs and macromolecules. The blind docking process includes a quest for binding sites on the entire surface of the macromolecule. The blind molecular docking of some recognized medications was screened with SARS-CoV-2 proteases along with some bioactive natural compounds. Docking of the protein targets and ligands was carried out by using Auto-Dock Vina (Trott and Olson, 2010) and the interaction of the protein-ligand complex was visualized using PyMOL and BIOVIA Discovery Studio 2020 (Dassault Systèmes BIOVIA, 2020).

2.5. Absorption, distribution, metabolism, excretion and toxicity (ADMET)

The prediction of the ADMET properties plays an important role in drug discovery and development. Properties such as ADMET of compounds were determined using SWISS ADME (http://www.swissadme.ch/) and are represented in supplementary table 2. The 2D representation of the compounds was downloaded from the PubChem database (Berman et al., 2000).

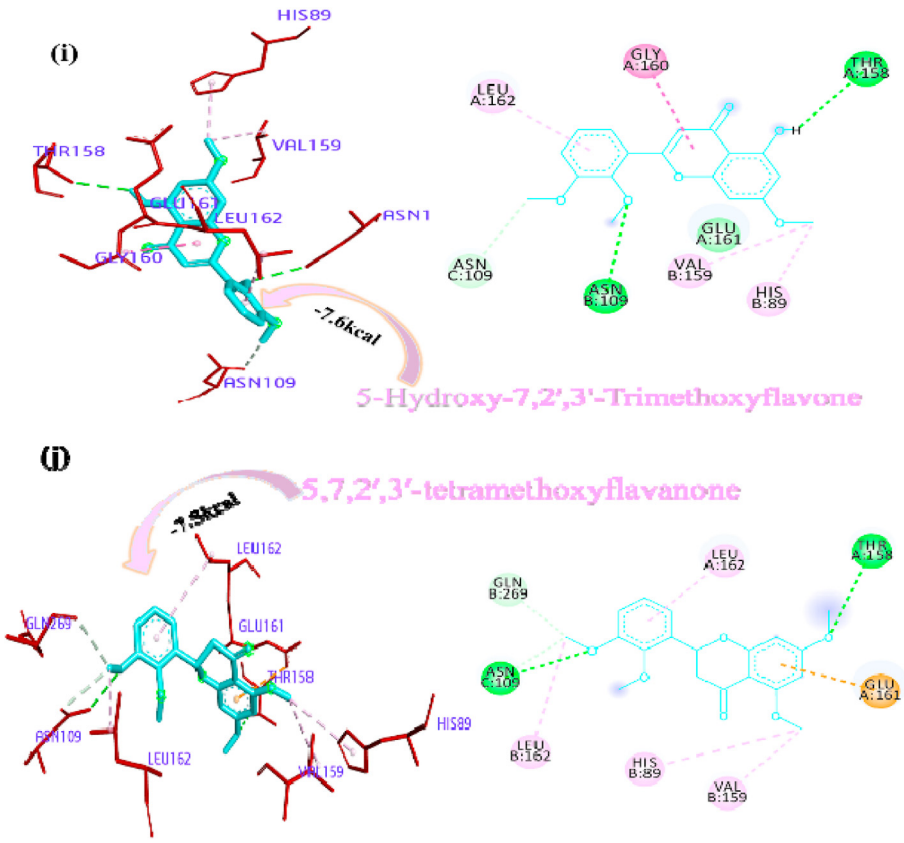

Fig. 1. (*continued*).

3. Ligand parameterization

Before performing the molecular dynamics simulation of protein-ligand complex, parameterization of ligand molecule is necessary to generate its topology and parameter files which would be used during the simulation of the complex system. For the parameterization of ligand, PRODRG2 server was used (Schüttelkopf and van Aalten, 2004).

4. Molecular dynamics (MD) simulation

Two complex structures containing canthin-6-one 9-O-beta-glucopyranoside (ligand) bound with 3-chymotrypsin-like protease (M^{pro}/$3CL^{pro}$) and papain-like protease (PL^{pro}) of SARS-COV-2 were taken to perform the MD simulation. All MD simulations were conducted using the GROMACS 5.12 MD (Páll et al., 2015) and GROMOS96 43a1 force field (van Gunsteren et al., 1996) implemented on Intel Xeon Quad Core W3530 2.8 8 M 1366 Processor with LINUX environment. The M^{pro}/$3CL^{pro}$ –ligand complex was solvated in a cubic box with a dimension of 9.96146 X 9.96146 × 9.96146 nm^3 while the PL^{pro}-ligand complex was solvated in a box with a dimension of 10.85766 X 10.85766 × 10.85766 nm^3. The simulation box of two complexes, M^{pro}/$3CL^{pro}$ –ligand and PL^{pro}-ligand showed to contain 31154 and 40531 SPC216 water molecules respectively (Miyamoto and Kollman, 1992). Four water molecules were replaced by Na^+ to neutralize the net charge of the complex system M^{pro}/$3CL^{pro}$ –ligand while for the neutralization of PL^{pro}-ligand complex 3 Cl^- were needed to replace solvent molecules. All protein atoms were maintained at a distance equal to 1.0 nm from the solvate box edges. The solvated systems were subjected to energy minimization for a maximum of 50000 steps by the steepest descent minimization method. After performing the energy minimization, both the minimized systems were equilibrated for 100 ps at 300K temperature by position restrained MD simulation in order to maintain the pressure and temperature of systems. Following equilibration, both the systems were subjected to a final production run of 100ns MD simulations at 300K temperatures. Periodic boundary conditions were applied under isothermal and isobaric conditions using Berendsen Coupling algorithm with a relaxation time of 0.1 and 0.2 ps, respectively (Weber et al., 2000). In both the systems, bond length was constrained using the LINCS algorithm at a time step of 2 fs (Hess et al., 1997). Particle Mesh Ewald method was used for the analyzing the electrostatic interactions. van der Waals and coulombic interactions were calculated with a cutoff at 1.0 nm (Darden et al., 1999). The tools provided by GROMACS program package such as RMSD, RMSF were utilized to analyse the MD trajectories. XMGrace (Vaught et al., 1996bib_Vaught_1996bib_Vaught_1996bib_Vaught_1996) program implemented in GROMACS was used to prepare the graphs.

5. Calculation of binding free energy

Binding affinity of the ligand canthin-6-one 9-O-beta-glucopyranoside in the docked complexes with the enzymes M^{pro}/$3CL^{pro}$ and PL^{pro} has been individually computed using a parallelized metadocking method implemented in the DINC server (Antunes, 2017). Coordinates of protein-ligand complexes as obtained from the MD simulation trajectories at an interval of 10 ns time scale were used for the calculation of binding energy. The working principle of the DINC server is based on the algorithm used in AutoDock-Vina. The grid center and dimension determined for each protein-ligand complex from the previous Autodock grid parameterization have been used during the calculation of binding energy.

6. MM-PBSA calculation

Molecular mechanics Poisson–Boltzmann surface area (MM-PBSA) calculation was performed for the canthin-6-one 9-O-beta-glucopyranoside bound M^{pro}/$3CL^{pro}$ and PL^{pro} system using the mmpbsa.py package implemented in GROMACS version 2018.1 (Kumari et al., 2014).

Fig. 1. (*continued*).

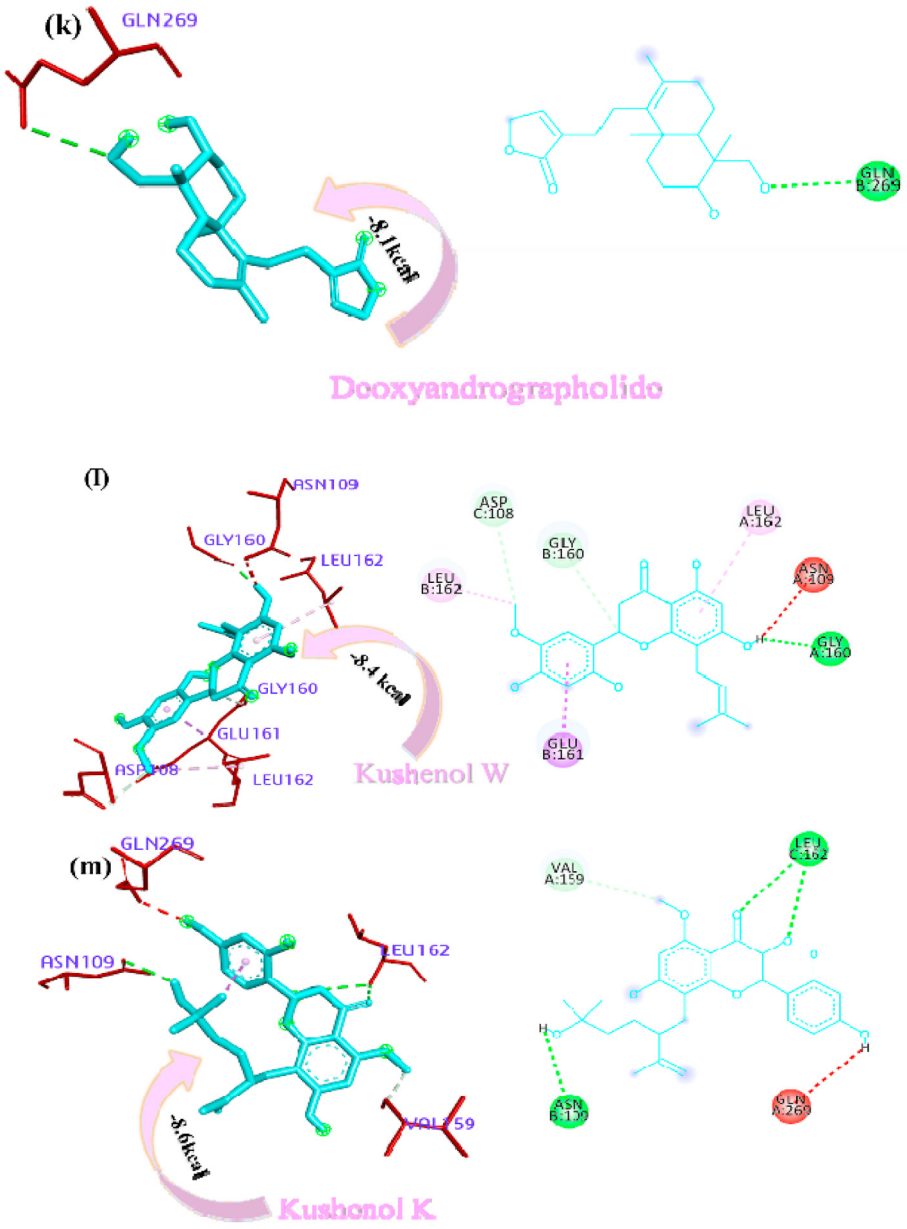

7. Result and Discussion

The novel coronavirus has a viral genome that encodes for the several proteins, which includes two proteases PL^{pro} and M^{pro}/$3CL^{pro}$ that play a crucial role in the viral life cycle and gained tremendous attention as a drug target. In the current study, these two proteases have been taken as a potential target. Eighteen phyto-compounds from the three medicinal plants viz. *E. harmandiana*, *S. flavescens* and *A. paniculate* were considered for the molecular docking analysis (Supplementary table 1). Chloroquine, oseltamivir, remdesivir and ribavirin has been used as a control. These drugs have been recently used in the treatment of COVID-19 patients and have been evaluated in clinical trials. There is no potential drug molecule approved by the FDA and this is the only reason that these repurposed drugs have been taken as a control in the current study. Oseltamivir in combination with hydroxychloroquine is also found to inhibit the coronavirus to some extent (Mitjà and Clotet, 2020; Wu et al., 2020). Remdesivir and ribavirin are the FDA-approved anti-RdRp drugs that were found through molecular docking approach (Pirzada et al., 2021; Hasan et al., 2021). Binding energies of various above-mentioned naturally occurring phytochemicals were obtained through Auto-Dock Vina. The interaction of inhibitor and protein receptor was predicted in 2D and 3D, with the help of BIOVIA Discovery study visualizer. The docked poses clearly showed that drug molecules and phyto-compounds bound to the active sites of SARS-COV-2 macromolecule structures.

7.1. Interaction with PL^{pro}

Panicoline bound firmly with the residue GLY^{160} through a conventional hydrogen bond, GLN^{269} through carbon-hydrogen bond and GLY^{160} *via*. van der Waals interactions with the surrounding residues of the PL^{pro} protein of SARS-CoV-2 (Fig. 1a). The 14-Deoxy-11,12-didehydroandrographolide stabilized the active site through conventional hydrogen bond (GLN^{269}), carbon-hydrogen bond (GLY^{160}) and van der Waals interactions with the rest of the residues (Fig. 1b). Canthin-6-one 9-O-beta-glucopyranoside appended within the active site of SARS-CoV-2 through pi-anion interaction with residues GLU^{161}, conventional hydrogen bond with residue LEU^{162}, GLY^{160}, ASN^{109}, Pi donor hydrogen bond with LEU^{162} and van der Waals interactions with the rest of the

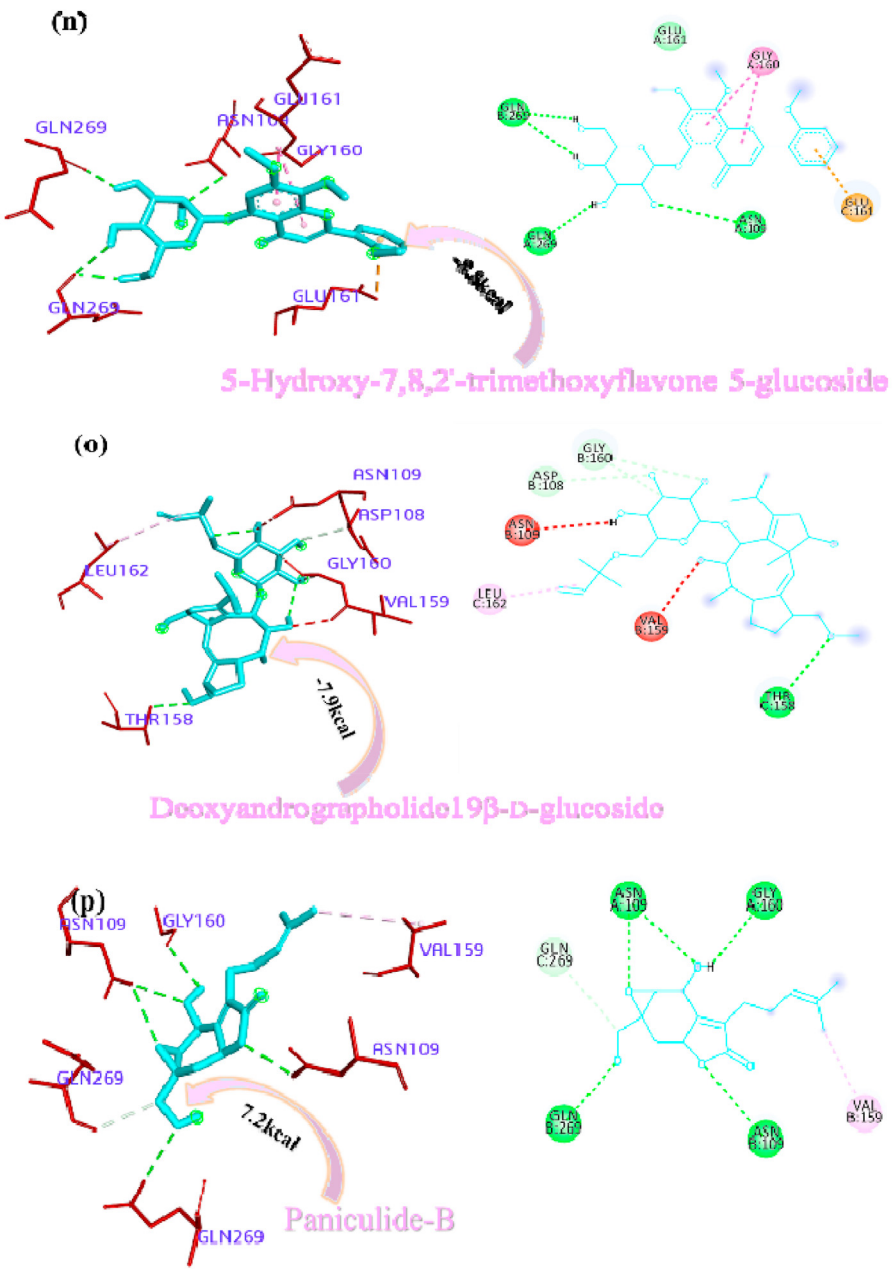

Fig. 1. (*continued*).

residues (Fig. 1c). Andrographine secured the active sites with amide-pi stacked interaction with residues GLY[161], conventional hydrogen bond with ASN[109], carbon hydrogen bond with ASP[108], pi-alkyl, alkyl interaction with the residues LEU[162], HIS[89], VAL[159] and van der Waals interactions with the surrounding residues (Fig. 1d). Andrographolide interacted with the active sites through conventional hydrogen bonds (VAL[159] and GLN[269]) and with van der Waals interactions with the rest of the residues as shown in Fig. 1e. 5-Hydroxy-7,8,2′,3′-Tetramethoxyflavone firmly stabilized the active sites through amide pi-stacked interaction with residues GLY[160], conventional hydrogen bond with ASN[109], carbon hydrogen bond with ASP108, GLN269, further it underwent alkyl, pi-alkyl interactions with residues LEU[162], VAL[159], HIS[89] and through van der Waals interactions with the rest of the residues (Fig. 1f). Neoandrographolide bound with the active sites through conventional hydrogen bonds (ASN[109], GLN[269], VA[159]) and carbon hydrogen bond (GLY[160], THR[158]) (Fig. 1g). Paniculide-A stabilized the active site of the PL[Pro] through alkyl interactions with residues VAL[159] and conventional hydrogen bond with residues ASN[109] (Fig. 1h). The 5-Hydroxy-7,2′,3′-Trimethoxyflavone bound with the active sites with residues LEU[162], VAL[159], HIS[89] through alkyl, pi-alkyl interactions, pi-anion interactions with residue GLY[160], conventional hydrogen bonds with residues THR[158], ASN[109] and carbon-hydrogen bond with residues ASN[109] and with rest of the residues through van der Waals interactions as shown in Fig. 1i. 5,7,2′,3′-tetramethoxyflavanone formed several noncovalent interactions at the active site, it formed a conventional hydrogen bond with THR[158], ASN[109], carbon-hydrogen bond with residue GLN[269], alkyl and pi-alkyl bond with LEU[162], HIS[89], VAL[159] and pi-anion interaction with residue GLU[161] (Fig. 1j). Deoxyandrographolide stabilized the active site only through a single conventional hydrogen bond (GLN269) and surrounding residues with van der Waals interaction (Fig. 1k). Kushenol W formed pi-sigma interactions with GLU[161], pi alkyl bond with LEU[162], conventional hydrogen bond with GLY[160], carbon-hydrogen bonds with residues ASP[108] and GLY[160] (Figure 1l). The kushenol K formed conventional hydrogen bonds with LEU[162], and ASN[109], carbon-hydrogen bond with VAL[159] and van der Waals interactions with the surrounding residues (Figure 1m). 5-Hydroxy-7,8,2′-

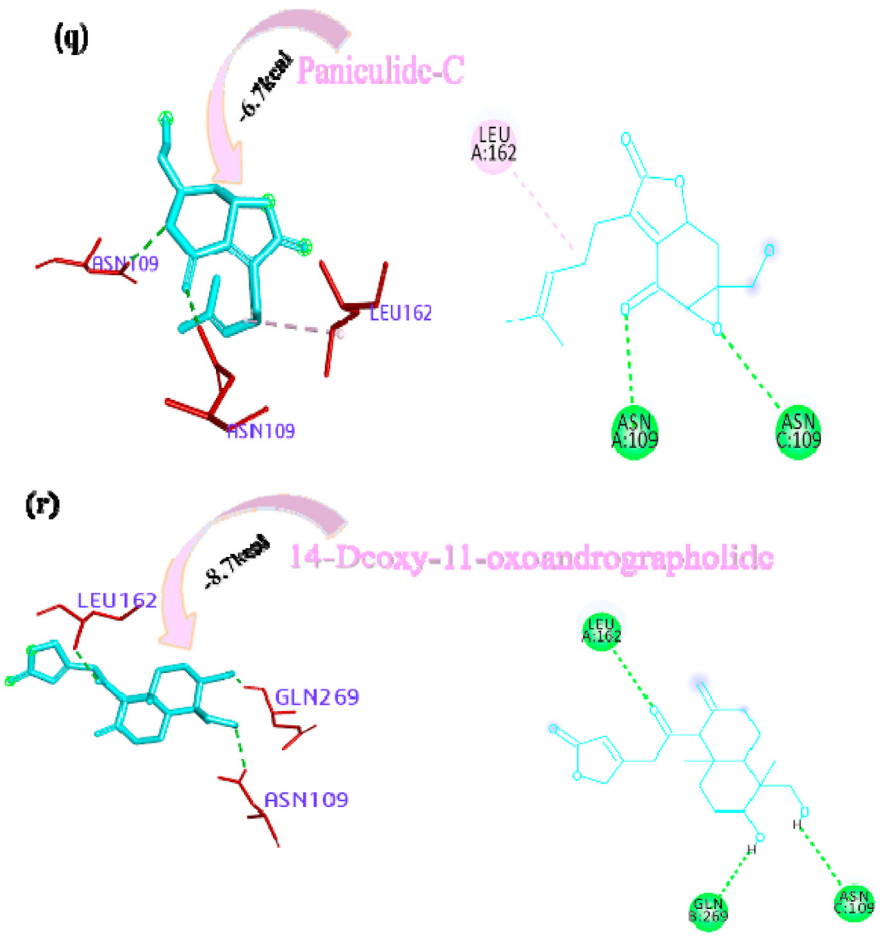

Fig. 1. (*continued*).

Table 1
Tabulated total free energy (kcal/mol) of docked protein PL^{pro}.

Compound name	Binding affinity (kcal/mol)
Canthin-6-one 9-O-beta-glucopyranoside	−9.4
5-Hydroxy-7,8,2′-trimethoxyflavone 5-glucoside	−8.8
14-Deoxy-11-oxoandrographolide	−8.7
Kushenol K	−8.6
Neoandrographolide	−8.6
Kushenol W	−8.4
14-Deoxy-11,12-didehydroandrographolide	−8.2
Deoxyandrographolide	−8.1
Paniculine	−8.0
Andrographolide	−7.9
Deoxyandrographolide19β-D-glucoside	−7.9
5-Hydroxy-7,8,2′,3′-Tetramethoxyflavone	−7.6
Andrographine	−7.6
5,7,2′,3′-tetramethoxyflavanone	−7.5
5-Hydroxy-7,2′,3′-Trimethoxyflavone	−7.5
Paniculide-A	−7.1
Paniculide-B	−7.2
Paniculide-C	−6.7

trimethoxyflavone 5-glucoside secured the active site through amide pi stacked interactions with residues GLY^{160}, pi-anion interaction with GLU^{161} and conventional hydrogen bond with GLN^{269}, and ASN^{109} (Figure 1n).

Deoxyandrographolide19β-D-glucoside bound active sites through a conventional hydrogen bond with residue THR^{158}, carbon hydrogen bonds with residues GLY^{160}, ASP^{108} and alkyl bond with residue LEU^{162} and it is depicted in form of 2D representation in Fig. 1o. Paniculide-B formed alkyl bond with VAL^{159}, conventional hydrogen bond with ASN^{109}, GLY^{160}, and GLN^{269}, and carbon hydrogen bond with GLN^{269} and where paniculide-C secured the active sites with alkyl (LEU^{162}), and conventional hydrogen bond (ASN^{109}) (Figure 1p and **q**). The interaction analysis of 14-Deoxy-11-oxoandrographolide depicted that it bound the active sites through conventional bond with residues LEU^{162}, ASN^{109} and GLN^{269} (Figure 1r).

Van der wall interactions and hydrogen bonds played a major role in the binding process. van der Waals interaction is the weakest intermolecular attraction between two molecules. Though it is the weakest bond between two atoms, a lot of van der Waals forces can make the interaction very strong (Barratt et al., 2005). In the protein-ligand interactions, the hydrogen bond helped the ligand to stabilize but there are also other interactions such as hydrophobic or van der Waals interactions that helped in stabilization of the nonpolar ligands too. An analysis of the structure of ligands and docked poses usually helped in understanding the interactions and the binding energy of the compounds. Based on these basics, the molecular docking program is the most widely used tool in the drug discovery process as the result suggested the potential drug compound based on the less affinity (Meng et al., 2011). The comparison of the estimated free energy of binding (ΔG) or binding affinity inferred that the canthin-6-one 9-O-beta-glucopyranoside (−9.4 kcal/mol) have the less affinity among the studied plant natural components and can be used as a potential drug candidate against the PL^{pro} of SARS-CoV-2 (Table 1).

The analysis of binding energies suggested that all the binding energy falls between −6.7 and 9.4 kcal/mol and 2D interaction in Fig. 1a-r depicted that the studied phyto-compounds have a lot of hydrogen bonds and van der Waals interactions that suggested that the ligands are stabilized within the complex.

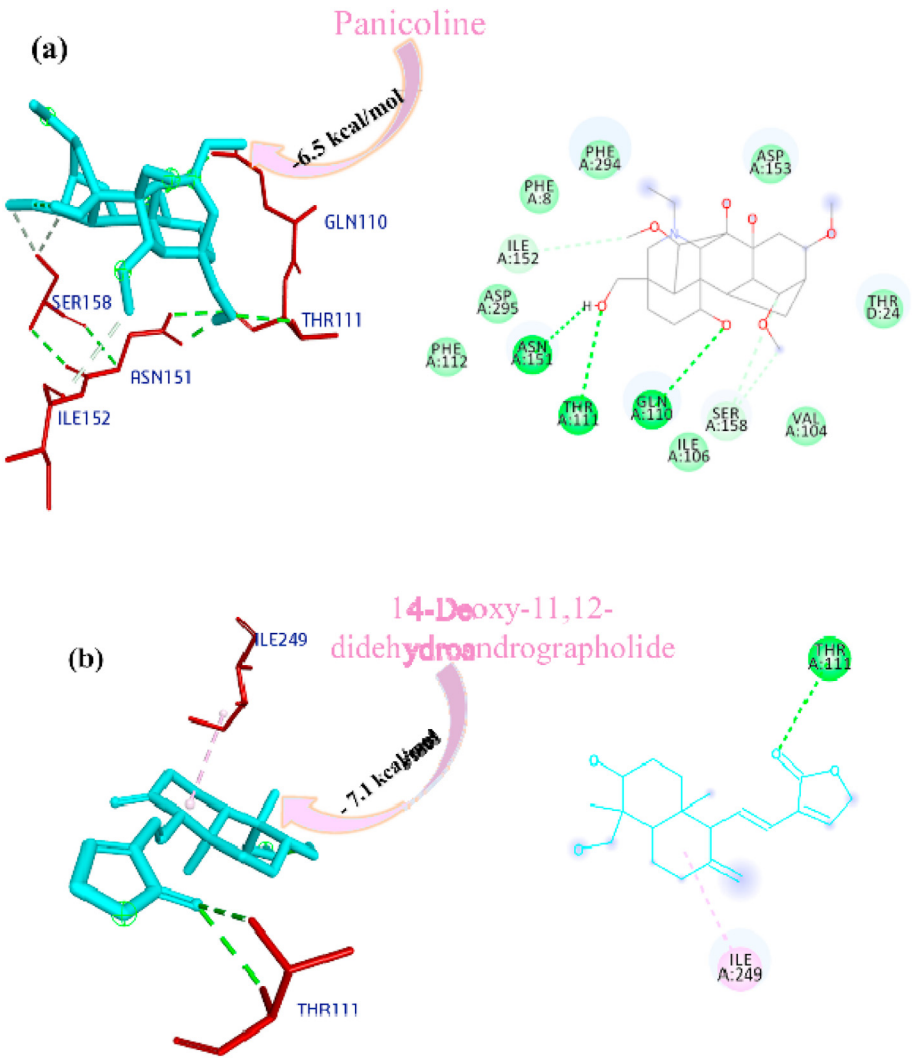

Fig. 2. Interactions established after docking the secondary metabolite against SARS-CoV-2 M^{pro}/$3CL^{pro}$ Protein (6M2N). The interacting residues of the protein are labeled in purple and the docking scores are listed under each of the complex, respectively. The receptor-ligand interaction is represented on a 3D diagram (Right) and 2D diagram (Left). Drugs are in cyan and interacting atoms of protein are represented red in the diagram, while green dotted lines represent the conventional h-bond interactions, light green dotted line represents weak van der Waals interactions. Additionally, dotted lines in sky blue display the pi-donor hydrogen bond, pi-sigma interaction is shown as violet dashed lines, pink dotted lines show alkyl and pi-alkyl interactions, respectively.

7.2. Interaction with M^{pro}/$3CL^{pro}$

Paniculine bound the active site of the main proteases (M^{pro} or $3CL^{pro}$) through hydrogen bonds and carbon hydrogen bonds with residues ASN^{151}, THR^{111}, GLN^{110}, SER^{158} and ILE^{152}, respectively (Fig. 2a). The 14-deoxy-11,12-didehydroandrographolide formed a hydrogen bond with residues THR^{111} and pi-alkyl interaction with ILE^{249} and van der Waals interaction with the surrounding residues (Fig. 2b). Canthin-6-one 9-O-beta-glucopyranoside firmly bound with the active site through conventional hydrogen bonds with residues THR^{111}, ASP^{295}, and THR^{292} and a pi-alkyl bond with VAL^{202} (Fig. 2c). Andrographine bound within the active sites through conventional hydrogen bond with the residue THR^{292}, pi-pi stacked interaction with the residue PHE^{294} and pi-alkyl bonds with PRO^{293} and ILE^{294} (Fig. 2d). Andrographolide formed conventional hydrogen bond with residue ASN^{151}, pi-sigma bond with residue PHE^{294} and van der Waals interaction with the surrounding residues (Fig. 2e). Neoandrographolide formed conventional hydrogen bond with the residues ASP^{295}, THR^{111} and pi alkyl interaction with residues VAL^{202}, PRO^{293} and ILE^{249} (Fig. 2f). Paniculide-A bound the active sites of the main protease (M^{PRO} or $3CL^{PRO}$) with conventional hydrogen bond and alkyl, pi-alkyl interactions with the residues GLN^{110}, THR^{111}, THR^{292} and ILE^{249}, PHE^{294}, PHE^{8}, respectively (Fig. 2g). 5-Hydroxy-7,8,2′,3′-Tetramethoxyflavone adhered to the active sites through conventional hydrogen bonds (ASN^{151} and THR^{111}), pi donor hydrogen bond (THR^{292}), pi-pi-stacked (PHE^{294}), pi-alkyl interactions with residues PRO^{293}, ILE^{294}, and PHE^{294}, depicted in Fig. 2h. 5,7,2′,3′-tetramethoxyflavanone formed Pi alkyl interactions, conventional hydrogen bonds pi-pi stacked interactions with residues ILE^{249}, THR^{111} and PHE^{294}, respectively (Fig. 2i). 5-Hydroxy-7,2′,3′-Trimethoxyflavone stabilized the active sites through conventional hydrogen bonds (ASN^{151} and THE^{111}), pi donor hydrogen bond (THR^{292}), pi-pi stacked interaction (PHE^{294}), alkyl, pi-alkyl interaction (PHE^{294}, ILE^{249}, HIS^{246} and PRO^{293}) and van der Waals interactions with the surrounding residues and the interactions can be seen in Fig. 2j. With a good efficiency of binding, deoxyandrographolide formed conventional hydrogen bond with ASN^{151} and pi-alkyl with PHE^{249} (Fig. 2k). Kushenol W bound with active sites residues THR^{111} through conventional hydrogen bond, pi-pi stacked interaction (PHE^{294}) and pi alkyl interactions (ILE^{249} and PRO^{293}) (Figure 2l). 5-Hydroxy-7,8,2′-trimethoxyflavone 5-glucoside formed conventional hydrogen bond with residue GLN^{110}, pi-sigma interaction (PHE^{294}), pi-pi interaction with PHE^{294}, alkyl, pi-alkyl interaction with VAL^{297}, PRO^{293}, ILE^{249} and carbon hydrogen bond with ILE^{249} (Figure 2m). Kushenol K stabilized the active site with residues PHE^{294} through pi-pi stacked interaction, pi-pi sigma interaction (ILE^{249}) and pi-alkyl interactions (PRO^{293} and PHE^{294}) (Figure 2n). The deoxyandrographolide19β-d-glucoside formed conventional hydrogen bond with residue THR^{21}, THR^{26}, GLN^{69}, ILE^{249} and carbon hydrogen bond with ASP^{245} (Figure 2o). Paniculide-B bound with the active sites through conventional hydrogen bonds (THR^{292}, THR^{111} and GLN^{110}) and alkyl interaction (PHE^{8} and PHE^{294}) whereas paniculide-C formed

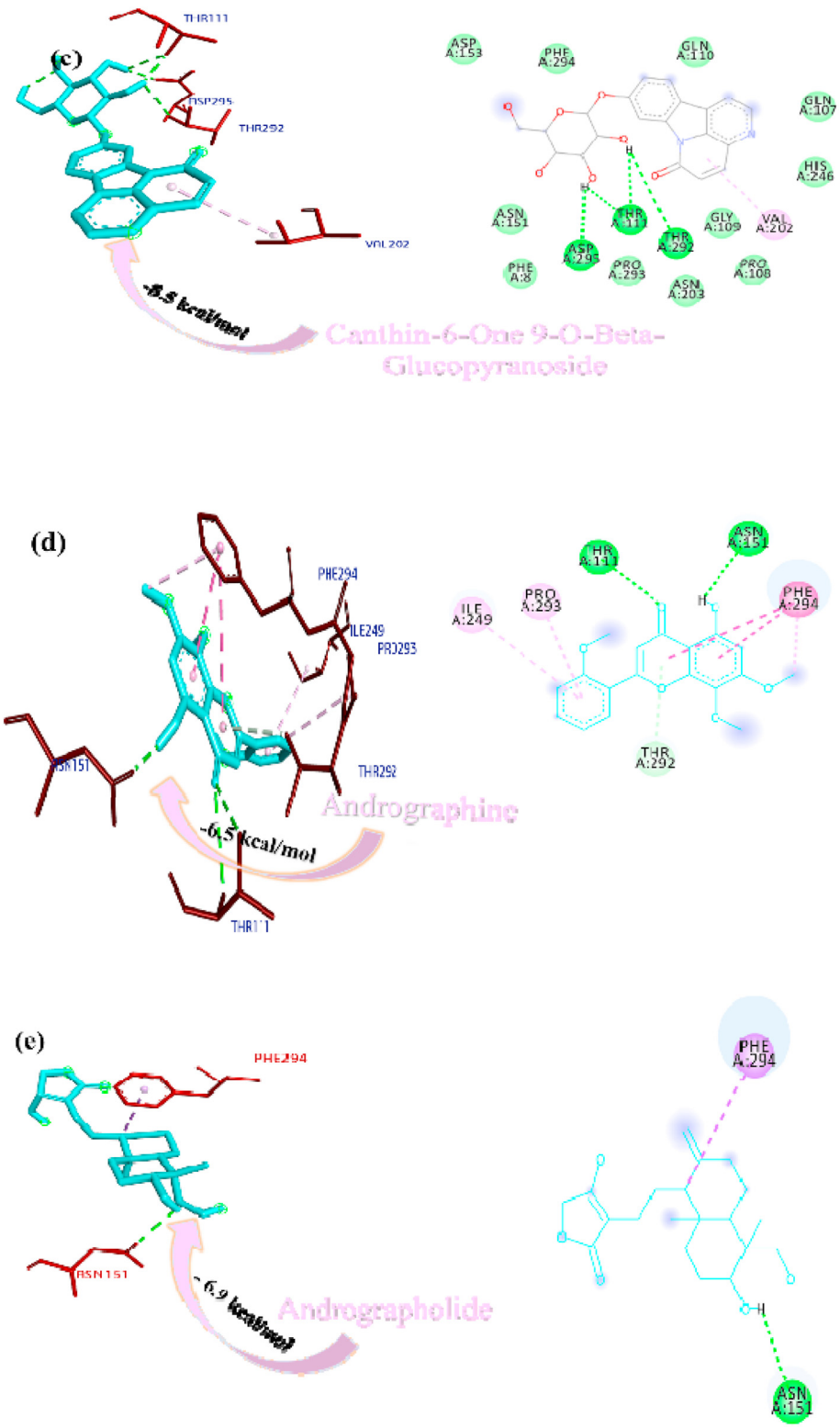

Fig. 2. (*continued*).

conventional hydrogen bonds with THR[111] and GLN[110]; alkyl and pi alkyl interactions with PRO[293], HIS[246], ILE[249], VAL[202] and the interactions are depicted in Fig. 2(p and q). In the case of 14-Deoxy-11-oxoandrographolide, it stabilized the active sites with residue GLN[269], ASN[109] and LEU[162] through conventional hydrogen bond, alkyl bond with ILE[249] and through van der Waals interaction with the rest of the residues (Figure 2r). The lower affinity of canthin-6-One 9-O-Beta-glucopyranoside (−8.5 kcal/mol) obtained from molecular docking study suggested that the molecule have good binding affinity against the M^{pro}/$3CL^{pro}$ (Table 2). The 2D and 3D interaction are depicted in Fig. 2 (a-r).

7.3. Interaction with control drugs

The docked pose of minimum energies conformers of four control drugs *viz.* chloroquine, oseltamivir, remdesivir and ribavirin [Fig. 3 (a-d)] showed chloroquine binds firmly with PL^{pro} active site and formed a

Fig. 2. (*continued*).

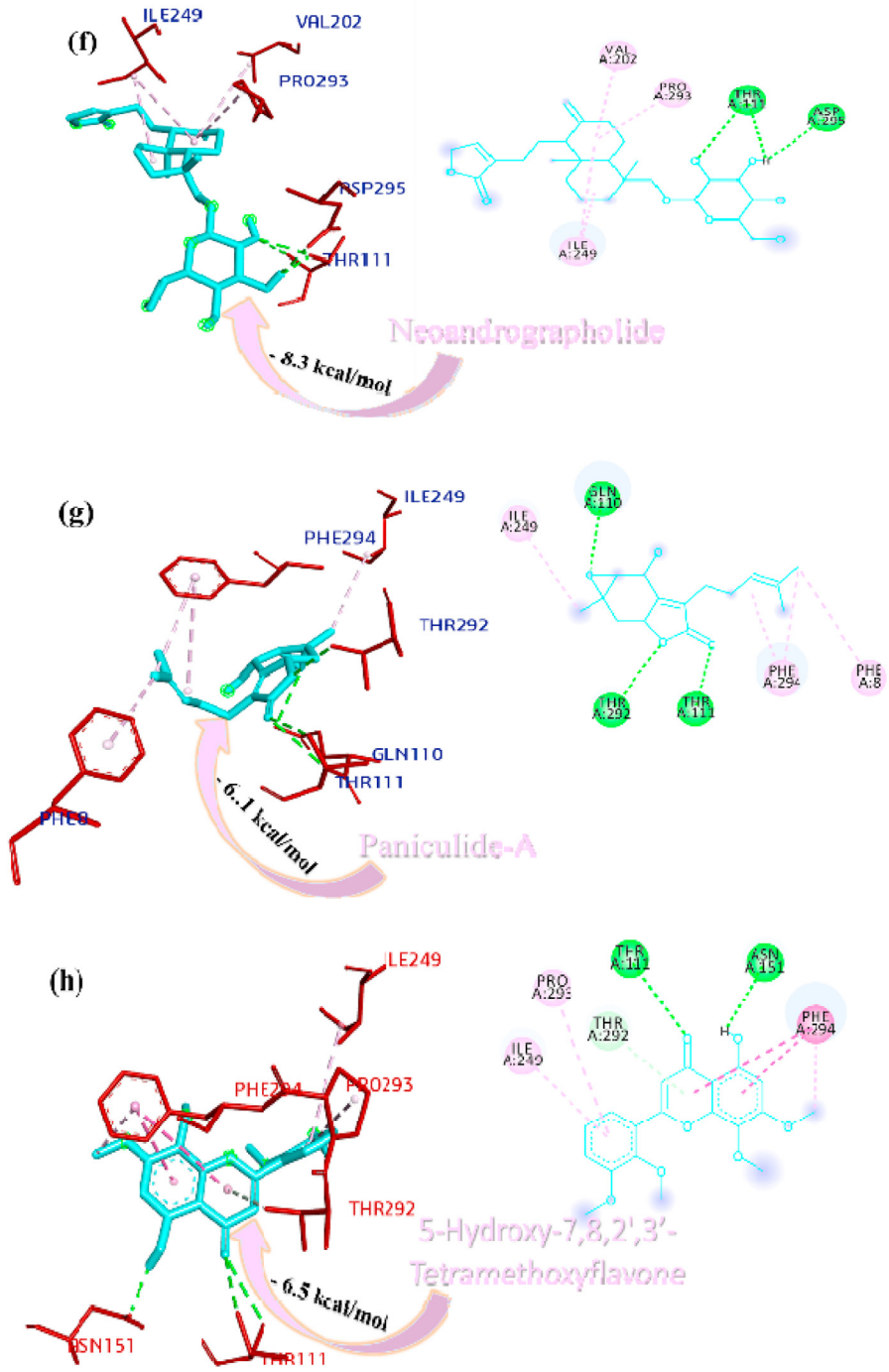

conventional hydrogen bond with THR^{158} residue and carbon-hydrogen bonds with residue GLU^{161} and VAL^{159}. Oseltamivir bound within the active site through conventional bonds with residue ASN^{109}, carbon-hydrogen bond with residue GLY^{160} and alkyl interaction with residue LEU^{162}. Remdesivir bound the active site through pi-anion (GLU^{161}), amide-pi stacked interaction (VAL^{159} and GLY^{160}), conventional a hydrogen bond (ASN^{109}) and pi-alkyl interaction (LEU^{162}). Ribavirin formed conventional hydrogen bond with residue GLY^{160}, GLN^{269}, LEU^{162}, and ASN^{109}, carbon-hydrogen bond with residue GLN^{269}, and ASN^{109} and among all the interactions van der waals interaction plays a major role. The comparison of binding affinity or estimated free energy (ΔG value) of binding showed that the remedisivir (−8.4 kcal/mol) have lower affinity with active sites of the PL^{pro}. The order of binding energy of other drugs with PL^{pro} is as follows: ribavirin (−6.8 kcal/mol) > oseltamivir (−6.4 kcal/mol) > chloroquine (−6.3 kcal/mol).

Interactions of the drugs with the M^{pro}/3CL^{pro} showed that chloroquine firmly bound within the active sites through pi-anion interaction with the residues ASP^{295}, pi-pi stacked interaction with residues PHE^{294} and pi-alkyl interaction with residue PHE^{294} and carbon-hydrogen bond with residue THR^{111}. It did not form any hydrogen bonds within the active site. Ribavirin formed a conventional hydrogen bond with residues GLN^{110}, PHE^{294}, THR^{111}, and THR^{292}. Oseltamivir stabilized the pi-alkyl interaction with PHE^{294} and conventional hydrogen bonds with residues GLN^{110}, THR^{111} and ASN^{151}. Remdesivir bound the active site through conventional hydrogen bonds (GLN^{110}, ASN^{151} and PHE^{294}) and pi-alkyl interaction (ILE^{249}, PRO^{252}, VAL^{297} and PRO^{293}) with the active sites of

Fig. 2. (*continued*).

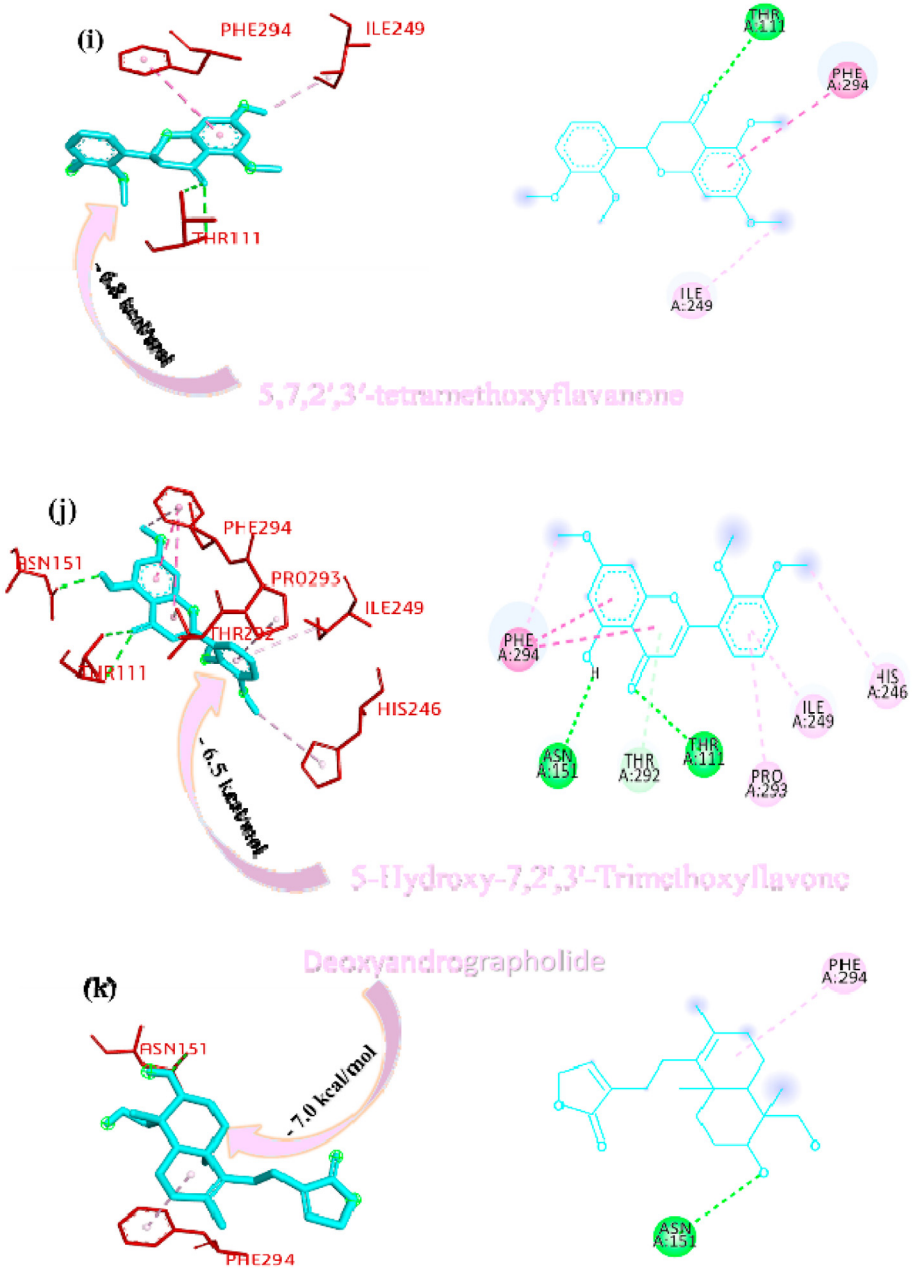

M^{pro}/$3CL^{pro}$. The pi-interaction played a major role instability of a particular drug within the active site (Arthur and Uzairu, 2019). The binding affinity of the drugs with M^{pro}/$3CL^{pro}$ suggested that the remdesivir have high affinity to inhibit the protein with most negative ΔG value *i.e.* - 8.3 kcal/mol and all the other studied drugs showed similar ΔG value i.e. −5.8 kcal/mol, the 3D and 2D interactions of drugs with the active sites of M^{pro}/$3CL^{pro}$ are depicted in Fig. 4 (a-d).

7.4. Pharmacokinetics

The prediction of the absorption, distribution, metabolism, excretion and toxicity (ADMET) properties played an important role in drug discovery and development. The absorption of drugs depends on membrane permeability, intestinal absorption, skin permeability levels, P-glycoprotein substrate or inhibitor. The distribution of drugs depends on factors that include the blood–brain barrier (logBB), central nervous system (CNS) permeability, and the volume of distribution (VDss). Metabolism is predicted based on the CYP models for substrate or inhibitors (CYP2D6, CYP3A4, CYP1A2, CYP2C19, CYP2C9, CYP2D6, and CYP3A4). Excretion is predicted which is based on the total clearance model and renal OCT2 substrate. The toxicity of drugs is predicted based on Ames toxicity, human ether-a-go-go-related gene (hERG) inhibition, hepatotoxicity, and skin sensitization. These parameters were calculated and checked for compliance with their standard ranges (Han et al., 2019). Properties such as ADMET profiling of compounds were determined using SwissADME, http://www.swissadme.ch/(Daina et al., 2017). Intestinal epithelium barrier/gut–blood barrier is a barrier that is a crucial barrier for all the compounds to overcome. Intestinal epithelium barrier regulates nutrients absorption, water and ion fluxes, and denotes the first defensive barrier against toxins and enteric pathogens and the gut-blood barrier (GBB) controls the passage of drugs from intestinal lumen to the bloodstream. Except, kushenol K, GI absorption of all the phytochemicals was high which means that it was predicted to be absorbed easily in gut and intestine epithelium. Distribution of compounds through various

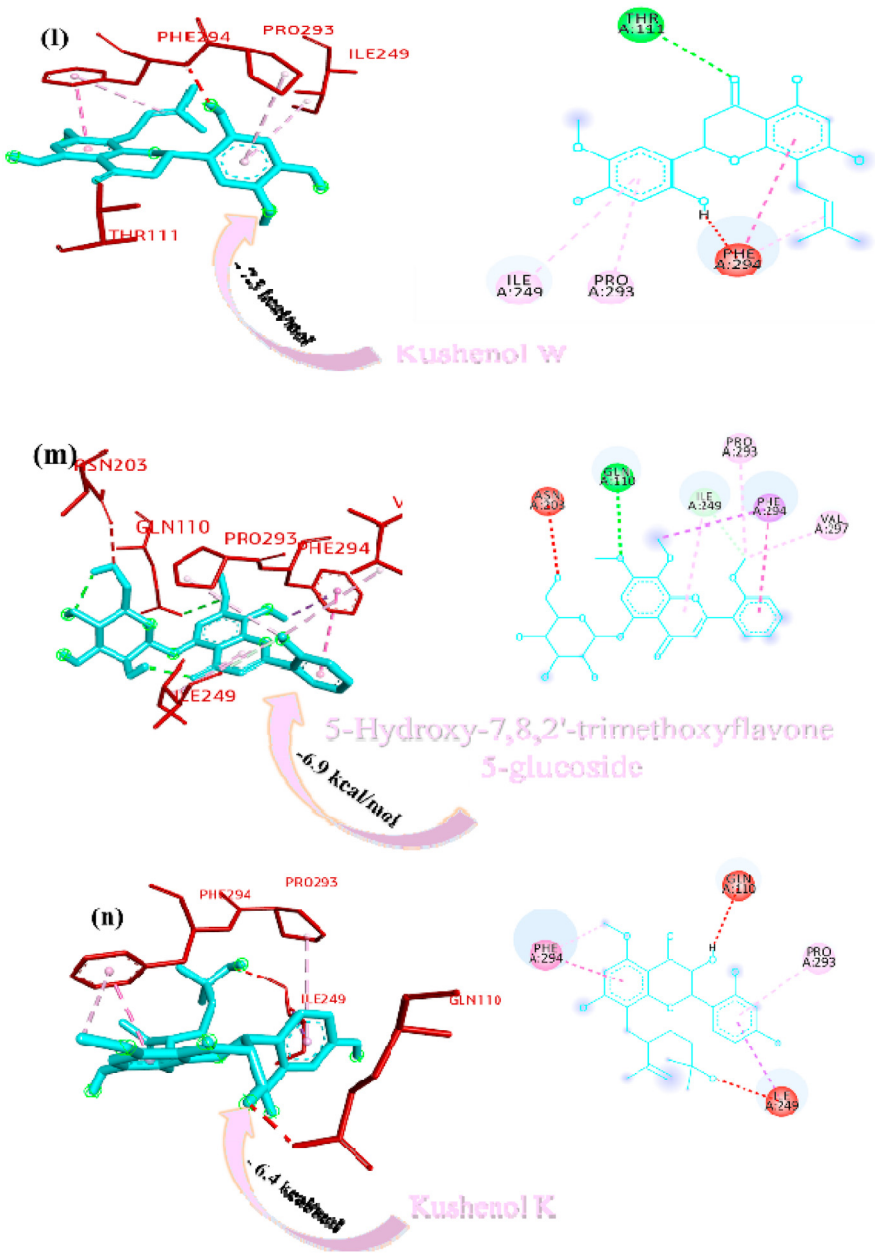

Fig. 2. (*continued*).

compartments of the body was accessed using its blood-brain barrier (BBB) penetration (Daneman and Prat, 2015). Among all the phyto-compounds, only panculide-A, andrographine, deoxyandrographolide, 5,7,2′,3′-tetramethoxyflavanone, 5-Hydroxy-7,2′,3′-Trimethoxyflavone were predicted to have blood brain barriers penetration. P-glycoprotein is a drug transporter having broad substrate specificity, drugs that are substrates of P-gp are subject to low intestinal absorption, low blood-brain barrier permeability, and face the risk of increased metabolism in intestinal cells. 14-deoxy-11,12-didehydroandrographolide, 5-hydroxy-7,8,2′-trimethoxyflavone 5-glucoside, andrographolide, paniculine A, neoandrographolide, kushenol K, 14-deoxy-11-oxoandrographolide, and deoxyandrographolide were predicted to have affinity for p-glycoprotein. The Result showed that except these phytochemicals, rest of the other phytochemicals may act as a non-substrate of p-glycoprotein (Pajouhesh and Lenz, 2005). Metabolism mainly depends on the CYP450 enzyme and its iso forms which are CYP 3A4, 2D6, 1A2, 2C9 and 2C19. These enzymes are responsible for the detoxification of drugs passing the liver. Therefore, any compound blocking P450 can cause toxicity. Out of all the 18 phyto-compounds, 5-hydroxy-7,8,2′-trimethoxyflavone 5-glucoside, neoandrographolide, kushenol W, kushenol K, andrographine, 5-Hydroxy-7,8,2′,3′-tetramethoxyflavone, 14-deoxy-11,12-didehydroandrographolide, 5,7,2′,3′-tetramethoxyflavanone, and 5-hydroxy-7,2′,3′-trimethoxyflavone compounds blocked the enzyme responsible for detoxification and hence, can be responsible for the toxicity. Skin permeation coefficient (log Kp) is the measure of skin to absorb a certain drug or chemical. In the given supplementary table 2, log kp of skin permeation of all the compounds lies between the standard value of log Kp −8.0 to −1.0 cm/s except 5-Hydroxy-7,8,2′-trimethoxyflavone 5-glucoside, deoxyandrographolide19β-D-glucoside, and paniculine, which showed that these possess an ability to absorb less in the membrane (Chen et al., 2018).

ADMET study of all these molecules suggested that the molecules canthin-6-one 9-O-beta-glucopyranoside, deoxyandrographolide 19β-d-glucoside or diterpene glucoside, paniculide-B, and paniculide-C have passed all the barriers of ADMET and indicated that these molecules can be a successful drug molecule. All these compounds have high gastrointestinal absorption which is an important and decision making standard of oral dosing, this implied that the phyto-compounds can be used as

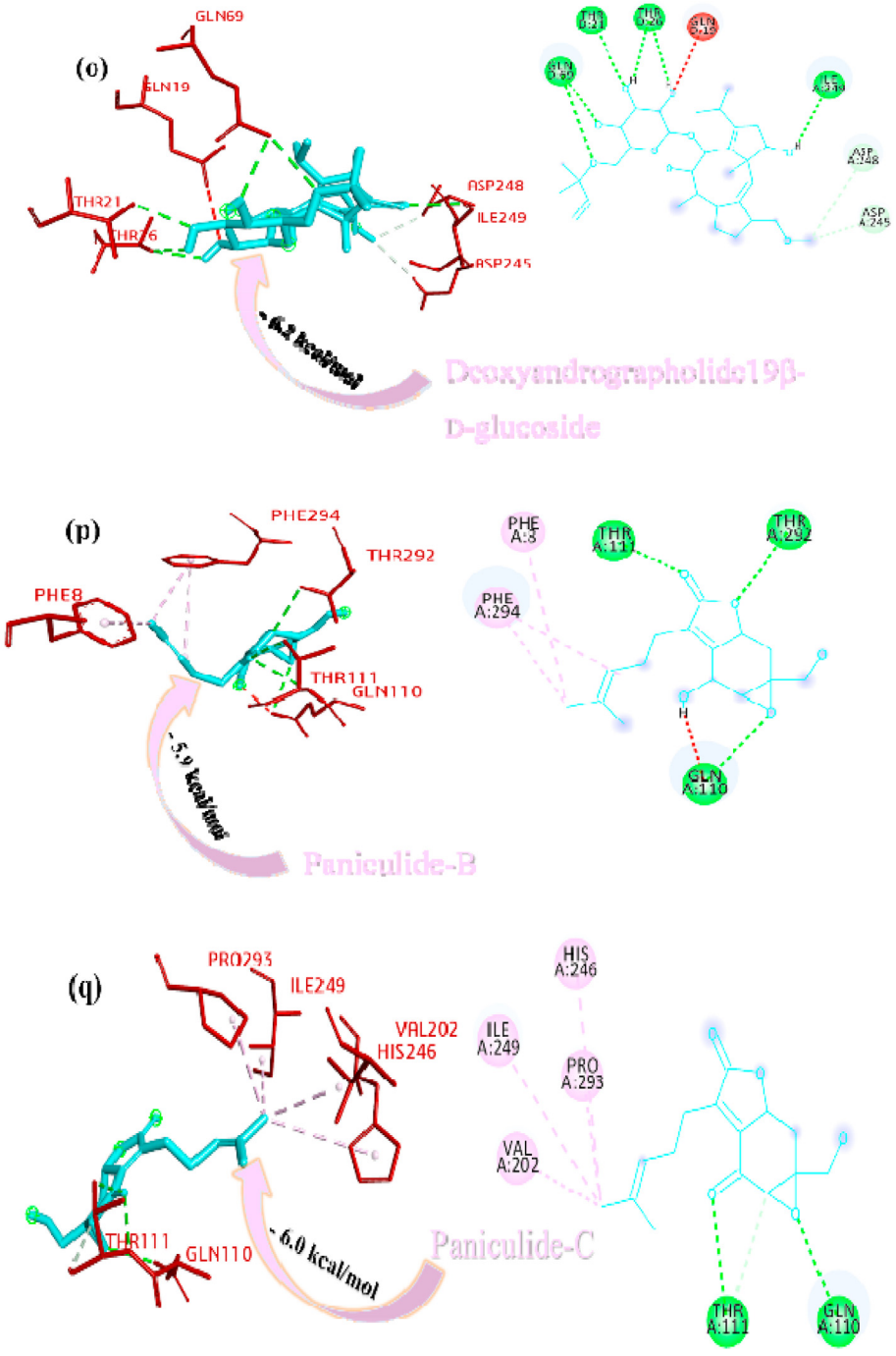

Fig. 2. (*continued*).

an oral drug. These drugs also passed the blood brain barrier (BBB) permeability test, therefore, these compounds qualify a fundamental index of drug distribution. High negative value of log Kp suggested that the phyto-compounds have less skin permeation. Binding of CYP450 enzyme may cause degradation of phyto-compounds inside the body and can lead to toxicity. Bioavailability of these compounds are high and it indicated high potential as drug molecule. The above mentioned parameters for all these molecules are in the range found for successful drug molecule (Supplementary table 2).

7.5. Potential drug against COVID 19

The molecular docking studies have been carried out using 18 phyto-compounds that might act as potential drug against SARS-CoV-2 M^{pro}/$3CL^{pro}$ and PL^{pro}. The analysis of molecular interaction between the active sites of the studied protein and the phyto-compounds suggested that these compounds can inhibit the protein and will block the viral replication. The active site of M^{pro}/$3CL^{pro}$ consists of residues THR^{21}, THR^{26}, GLN^{69}, GLN^{110}, THR^{111}, ASN^{151}, HIS^{246}, ILE^{249}, THR^{292} and ASP^{295} whereas the active site residues for PL^{pro} are ASN^{109}, THR^{158}, VAL^{159}, GLY^{160}, LEU^{162} and GLN^{269} (Supplementary table 3). The canthin-6-one 9-O-beta-glucopyranoside in comparison with the control drugs, showed lower affinity with active sites of both the target proteins i.e. M^{pro}/$3CL^{pro}$ and PL^{pro}. The distance between the ligand and catalytic residues of the protein showed that the canthin-6-one 9-O-beta-glucopyranoside interacted within the active site of the protease proteins and have high affinity of binding. The ADMET study also suggested that the canthin-6-one 9-O-beta-glucopyranoside have all the drug like properties

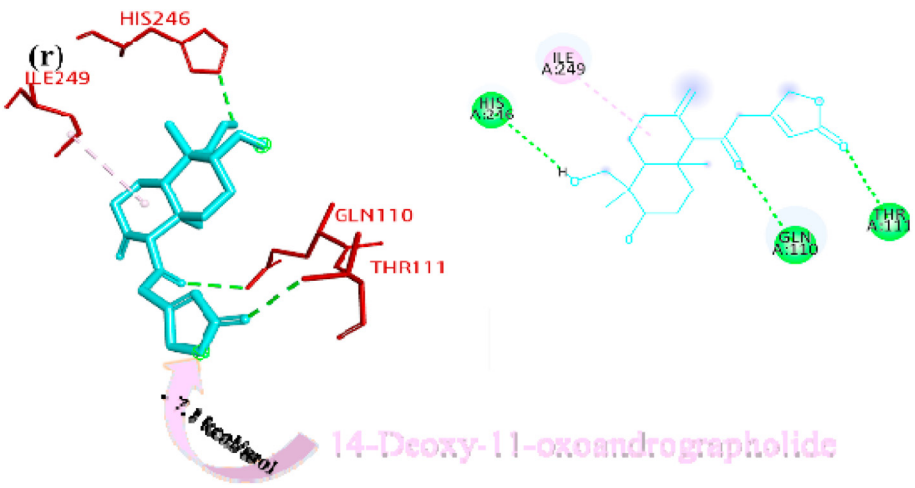

Fig. 2. (*continued*).

Table 2
Tabulated total free energy (kcal/mol) of docked protein M^{pro}/$3CL^{pro}$.

Compound name	Binding affinity (kcal/mol)
Canthin-6-One 9-O-Beta-Glucopyranoside	−8.5
Neoandrographolide	−8.4
Kushenol W	−7.3
14-deoxy-11,12-didehydroandrographolide	−7.1
14-deoxy-11-oxoandrographolide	−7.1
5-hydroxy-7,8,2′-trimethoxyflavone 5-glucoside	−6.9
Andrographolide	−6.9
5-hydroxy-7,2′,3′-trimethoxyflavone	−6.8
5,7,2′,3′-tetramethoxyflavanone	−6.5
5-hydroxy-7,8,2′,3′-tetramethoxyflavone	−6.5
Andrographine	−6.5
Paniculine	−6.5
Kushenol K	−6.4
Deoxyandrographolide19β-d-glucoside	−6.2
Diterpene glucoside	−6.2
Paniculide-A	−6.1
Paniculide-B	−5.9
Paniculide-C	−6.0

and can be considered as a potential drug against the infection caused by SARS-CoV-2.

8. MD simulation

8.1. Root mean Square deviation (RMSD)

Structural changes specifically the deviation between two structures can be best interpreted by using the graph obtained after calculating RMSD from the MD simulation trajectories. This calculation can determine the spatial differences between the backbone atoms present in the protein throughout the simulation time. The differences are calculated in respect with the initial structure at the start of the simulation. The smaller the differences, the more spatially equivalents the compared structures are, whereas more distantly related structures are defined by comparatively greater RMSD values. Thus, a greater RMSD value indicates the instability of a protein system.

Comparative RMSD pattern analysis between canthin-6-One 9-O-beta-Glucopyranoside bound M^{pro}/$3CL^{pro}$ and PL^{pro} protein complexes demonstrated that, both complexes showed a more or less similar RMSD values up to first 19 ns of MD trajectory. After 19 ns of MD simulation, there is a comparative more deviation observed in case of PL^{pro} protein than M^{pro}/$3CL^{pro}$ up to 32 ns time scale of MD simulation. After 32 ns and up to next 3 ns time scale of MD trajectory, relatively less RMSD has been recorded for PL^{pro} protein than from M^{pro}/$3CL^{pro}$ when interacting with canthin-6-One 9-O-beta-Glucopyranoside. Again a greater RMSD value of PL^{pro} protein backbone has been shown for next 13 ns and up to 48 ns of MD simulation compared to M^{pro}/$3CL^{pro}$ protein. From 48 ns to 100 ns of MD simulation, the backbone of PL^{pro} protein deviated less than in case of M^{pro}/$3CL^{pro}$ protein (Supplementary Figure 1). The Result indicated that M^{pro}/$3CL^{pro}$ and PL^{pro} protein have the occasional backbone stability throughout the MD simulation while bound with the ligand Canthin-6-One 9-O-beta-Glucopyranoside.

8.2. Root mean Square Fluctuation (RMSF)

A more detailed view of differences in residue mobility in both the M^{pro}/$3CL^{pro}$ protein and PL^{pro} bound with ligand canthin-6-One 9-O-beta-Glucopyranoside has been obtained from the RMSF graph calculated for the Cα atoms in comparison with the respective average structure of the two complexes throughout the simulation. RMSF values increases with the depletion of secondary structure of a protein that sometime may be caused due to the decline in binding affinity between the protein and ligand. It has been noted that the ligand binding residue in M^{pro}/$3CL^{pro}$ Asn203 has the minimum RMSF value of 0.0881 among the 5 interacting residues of canthin-6-One 9-O-beta-Glucopyranoside while in PL^{pro} protein, the residue Asn109 has the minimum RMSF value of 0.1038 among the 3 interacting residues with the ligand (Supplementary Figure 2; Supplementary table 4).

This relative Result from RMSF analysis revealed that Asn203 residue of the protein M^{pro}/$3CL^{pro}$ might have greater impact for a tight binding with the ligand canthin-6-One 9-O-beta-Glucopyranoside in compare with the residue Asn109 in PL^{pro} protein as the residue Asn203 has comparatively lower RMSF value than that of Asn109. Bharatiy et al. (2016) has studied some stabilizing and destabilizing saltbridge forming residues of two homologues mesophilic and thermophilic α-carbonic anhydrase (α-CA) from *Neisseria gonorrhoeae* and *Sulfurihydrogenibium* sp. on aspect of their respective RMSF value. Likewise, as the result from the present study, Bhartiy et al. (2016) also reported about some salt bridge residues having notably less RMSF values in maintaining higher conformational stability of *Sulfurihydrogenibium* sp. α-CA at higher temperature compared to its mesophilic counterpart.

8.3. Free energy calculations

Comparative binding calculation between M^{pro}/$3CL^{pro}$ and PL^{pro} bound with ligand Canthin-6-One 9-O-beta-Glucopyranoside throughout the 100 ns MD simulation presented that, the protein M^{pro}/$3CL^{pro}$ has comparatively more affinity with the ligand in relation to PL^{pro} at most of the time scale in MD simulation. Binding energy calculation at the start of the simulation between two complexes of canthin-6-One 9-O-beta-

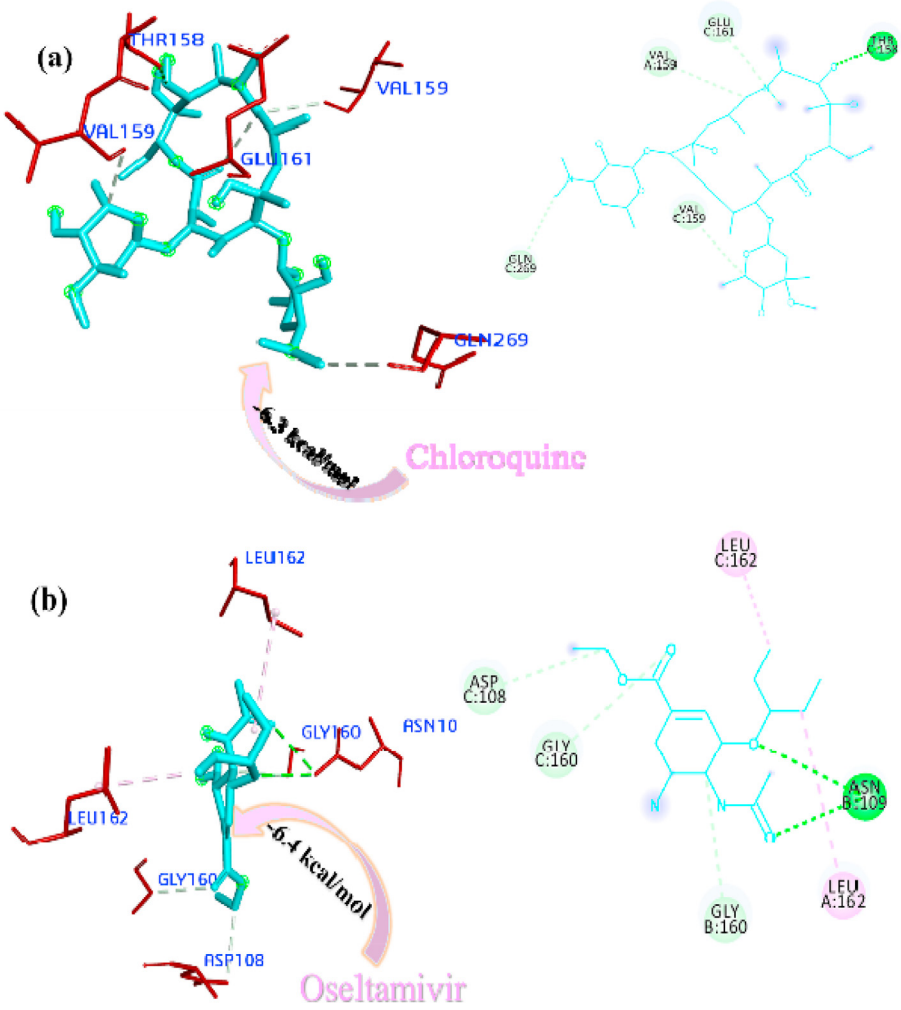

Fig. 3. Interactions established after docking the drugs against SARS-CoV-2 PL^{pro} protein (6W9C). The receptor-ligand interaction is represented on a 3D diagram (Right) and 2D diagram (Left). The interacting residues of the protein are labeled in purple and the docking scores are listed under each of the complex, respectively. Drugs are in cyan and interacting atoms of protein are represented red in the diagram, while green dotted lines represent the conventional h-bond interactions, light green dotted lined represents weak van der Waals interactions. Additionally, dotted lines in sky blue display the pi-donor hydrogen bond, pi-sigma interaction is shown as violet dashed lines, pink dotted lines show alkyl and pi-alkyl interactions, respectively.

Glucopyranoside bound M^{pro}/$3CL^{pro}$ and PL^{pro} revealed that the M^{pro}/$3CL^{pro}$ protein has an affinity value of −8.70 kcal/mol which is much higher than that of PL^{pro} with a value of −4.80 kcal/mol. While at the next two 10 ns time scale intervals, PL^{pro} showed higher binding affinity (−8.20 and −5.40 kcal/mol) with the ligand in comparison to M^{pro}/$3CL^{pro}$ (−5.80 and −4.20 kcal/mol). Interestingly, at 30 ns and 40 ns of time scale in MD simulation, again M^{pro}/$3CL^{pro}$ protein exhibited comparative greater binding affinity (−5.00 and −5.20 kcal/mol) compared to PL^{pro} (−3.40 and −4.90 kcal/mol). At 50 ns, a relatively higher binding energy towards ligand has been recorded for PL^{pro} with a value of −8.10 kcal/mol than in the case of M^{pro}/$3CL^{pro}$ with a value of −7.60 kcal/mol. Significant difference in binding energy between M^{pro}/$3CL^{pro}$ and PL^{pro} has been reported while interacting with the ligand at the time scale of 60 ns, 80 ns and 90 ns in MD simulation. For the protein M^{pro}/$3CL^{pro}$ binding energy values of −9.80, −9.00 and −10.50 kcal/mol has been calculated in place of −3.40, −3.60 and −3.60 kcal/mol for PL^{pro} respectively at those three time scales. After the completion of the 100 ns MD simulation, a greater binding energy of −10.00 kcal/mol has been documented for M^{pro}/$3CL^{pro}$ towards the ligand canthin-6-one 9-O-beta-glucopyranoside while for PL^{pro} a value of −8.20 kcal/mol was recorded (Fig. 5).

Binding energy *vs.* RMSD plots have been graphically represented for M^{pro}/$3CL^{pro}$ and PL^{pro} while interacting with the ligand canthin-6-one 9-O-beta-glucopyranoside at 10 ns time interval up to 100 ns MD simulation (Fig. 6). Comparative higher binding affinity of M^{pro}/$3CL^{pro}$ with the ligand than PL^{pro} is also might be resulted from the relatively less flexible residue Asn203 present in the protein M^{pro}/$3CL^{pro}$ which has lower RMSF value as compare to Asn109 of PL^{pro} that was determined previously. Thus, the overall Result from this binding energy analysis suggested that, M^{pro}/$3CL^{pro}$ has remarkably greater binding affinity and hence stronger interaction with the ligand canthin-6-one 9-O-beta-glucopyranoside than PL^{pro} throughout most of the time scales in their dynamics state.

8.4. MM-PBSA interaction energy

From the MM-PBSA calculation, it can be observed that in case of canthin-6-One 9-O-beta-Glucopyranoside bound with M^{pro}/$3CL^{pro}$, there is comparatively higher degree of energy contribution than in the case of PL^{pro} bound complex of the same ligand (Fig. 7). This observation is in agreement with the Result found from the previously performed RMSD vs. binding energy plots for the two protein complexes where M^{pro}/$3CL^{pro}$ presented higher binding affinity towards the ligand canthin-6-One 9-O-beta-Glucopyranoside. Shahbaaz et al. (2017), in their study has performed the same kind of MM-PBSA analysis for the protein Rab21 GTPase during the interaction with both the GDP and GTP through 50ns MD simulation. In their study, comparatively greater energy contribution has been recorded for the ligand GTP than the GDP during their interaction with Rab21 GTPase.

Das et al. (2020) studied 33 molecules through the help of docking approach, and find out that these molecules could bind near the Cys^{145} and His^{41} (catalytic residue) of the main protease. Salim and Noureddine

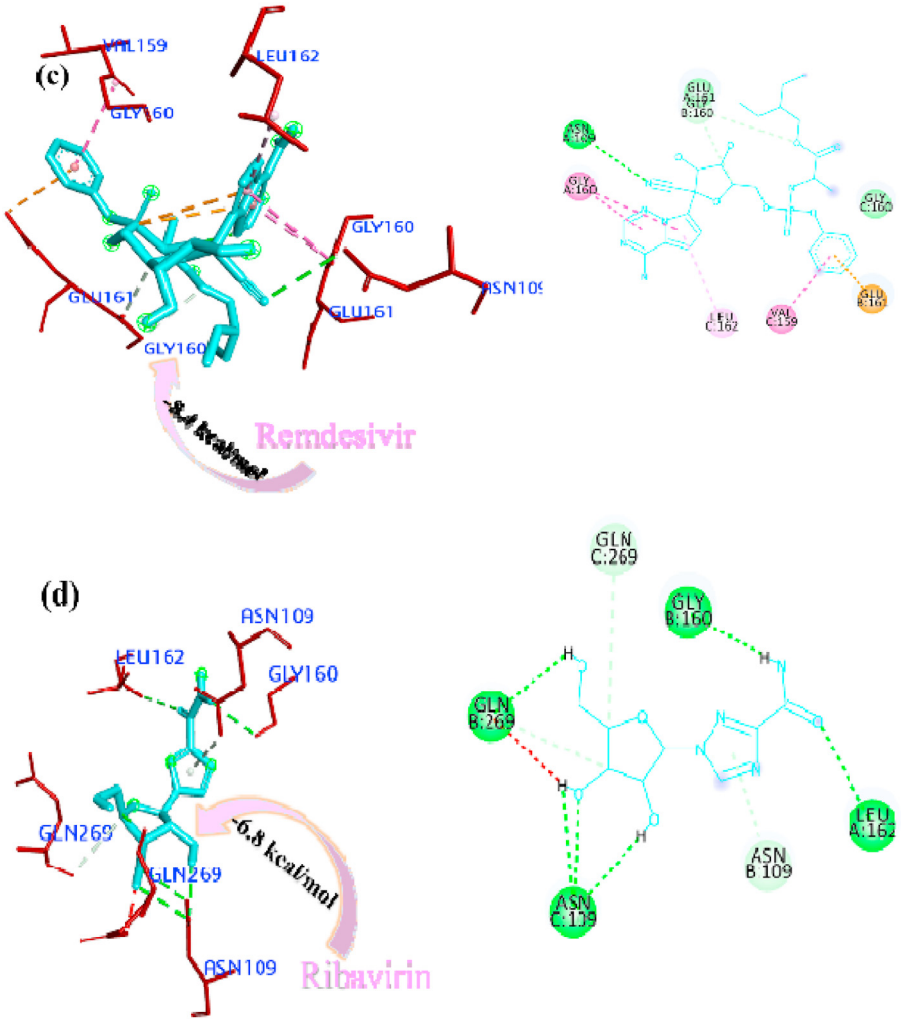

Fig. 3. (*continued*).

(2020) reported that α-hederin and nigellidine are the major phytochemical obtained from *Nigella sativa* which are capable of restricting SARS-CoV-2 with great energy score as compared to clinical drugs based on molecular docking. Muralidharan et al. (2020) performed MD simulations to evaluate the interconnection among the protein and three drugs. The RMSD of interconnection is found to be 3 Å and remain firm while the simulations. Therefore, the amalgam of ritonavir, lopinavir, and oseltamivir are greatly efficacious against the protease of SARS-CoV-2, and these agents can be surveyed further for drug reusing purposes for the victorious restriction of SARS-CoV-2. Joshi et al. (2020) identified some natural compounds such as phyllaemblicin B, hesperidin, biorobin, afzelin, nympholide A, lacticopicrin 15-oxalate, myricitrin, nympholide A, and d-viniferin from the screening of ~7100 molecules which proved as a strong binders not only for proteases but also for other targets (RNA dependent RNA polymerase, and human angiotensin-converting enzyme of SARS-CoV-2. Adeoye et al. (2020) determined the inhibitory potentiality of chloroquine, lopinavir, remdesivir, ribavirin, azithromycin, and oseltamir towards viral proteases, V-ATPase, SARS-CoV spike glycoprotein/ACE-2 complex, and protein kinase A. It was evaluated that, lopinavir has the greatest affinities for the 3-chymotrypsin like protease, cyclic AMP-dependent protein kinase A, and SARS-CoV spike glycoprotein/ACE-2 complex whereas remdesivir has shown affinities for papain-like proteins, and vacuolar proton-translocating (V-ATPase), and chloroquine has affinities for cyclic AMP-dependent protein kinase A, and 3-chymotrypsin-like protease in comparison to ribavirin and oseltamivir (McKee et al., 2020). Aanouz et al. (2020) used the docking process for examining the interaction type and affinity at the binding site among the 67 compounds and the SARS-CoV-2 proteases. The results showed that, only three molecules (b-eudesmol, crocin, and digitoxigenin) are found as inhibitors in the control of SARS-CoV-2. Enmozhi et al. (2020) evaluated andrographolide from *A. paniculata* as a main protease inhibitor in case of SARS-CoV-2 through *in silico* studies. Kumar et al. (2020a, b) carried out molecular docking study of FDA approved drugs that are used in the cure of different viral ailments in order to investigate their binding affinity for the active site of M^{pro} (Lobo-Galo et al., 2020). Docking studies determined that drugs raltegravir, tipranavir, and lopinavir-ritonavir among others particularly binds to the proteases with similar affinity as of the α-ketoamide inhibitors (Muralidharan et al., 2020). From the earlier time, herbal plant products are successfully employed for the cure of several viral disorders (Mukhtar et al., 2008; Lin et al., 2014). Many of the promising lead natural compounds of our investigation are anti-viral, therefore, there is a big probability that these bioactive constituents would be appropriate in the control of SARS-CoV-2 and could be helpful for the discovery of multi-targeted agent against the SARS-CoV-2 infection (Sharma et al., 2020; Jyotisha et al., 2020; Vimal et al., 2020; Ribaudo et al., 2020).

The hunt for plant-derived antiviral for the control of SARS-CoV-2 is hopeful, as many plants have been reported to be effective against beta coronaviruses (Mitra et al., 2021; Tallei et al., 2020; Chowdhury et al., 2020; Babar et al., 2020; Gideon A. Gyebi et al., 2020; Yepes-Pérez et al., 2020; Lakshmi et al., 2020; Razzaghi-Asl et al., 2020; Subhomoi and Banerjee, 2020). Many reports to recognize the promising inhibitors of SARS-CoV-2 from plants have been published by using a computational

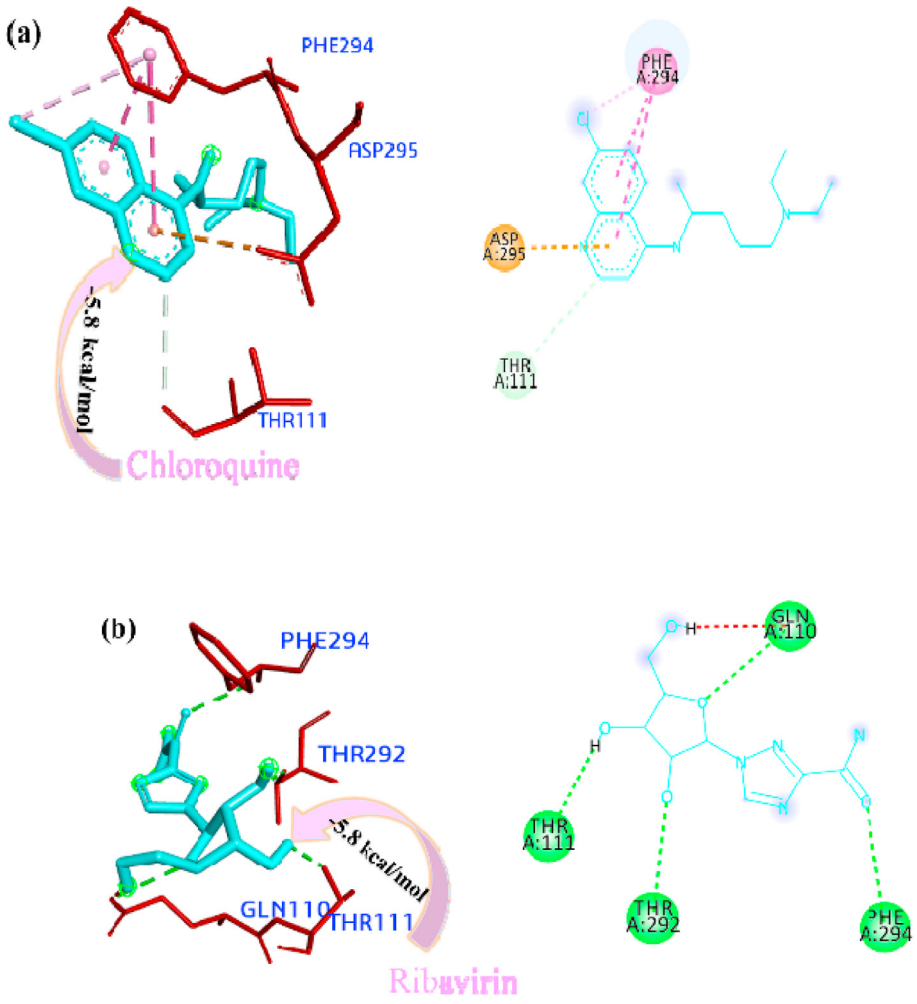

Fig. 4. Interactions established after docking the drugs against SARS-CoV-2 M^{pro}/$3CL^{pro}$ Protein (6M2N). The interacting residues of the protein are labeled in purple and the docking scores are listed under each of the complex, respectively. The receptor-ligand interaction is represented on a 3D diagram (right) and 2D diagram (left). Drugs are in cyan and interacting atoms of protein are represented red in the diagram, while green dotted lines represent the conventional h-bond interactions, light green dotted lined represents weak van der Waals interactions. Additionally, dotted lines in sky blue display the pi-donor hydrogen bond, pi-sigma interaction is shown as violet dashed lines, pink dotted lines show alkyl and pi-alkyl interactions, respectively.

approach (Pant et al., 2020; Elmezayen et al., 2020; Ghosh et al., 2020; Das et al., 2020; Maroli et al., 2020; Shree et al., 2020; Saravanan et al., 2020; Toluwase Hezekiah Fatoki et al., 2020; Rolta et al., 2020; Aanouz et al., 2020; Vimal et al., 2020). In the present study, after evaluating the multiple medicinal properties of the natural products, a total 18 compounds (canthin-6-one 9-O-beta-glucopyranoside from *E. harmandian;* kushenol W, and kushenol K from *S. flavescens*; and 3α, 14, 15, 18-Tetrahydroxy-5β, 9βH, 10α-labda-8, 12-dien-16-oic acid γ-lactone, deoxyandrographolide, neoandrographolide, 14-deoxy-11, 12-didehy droandrographolide, deoxyandrographolide19β-d-glucoside, 5,7,2′, 3′-tetramethoxyflavanone, 5-hydroxy-7,2′,3′-trimethoxyflavone, 14-deo xy-11-oxoandrographolide, 5-hydroxy-7,8,2′,3′-tetramethoxyflavone, 5-hydroxy-7,8,2′, trimethoxyflavone, andrographine, panicoline, paniculide-A, paniculide-B, and paniculide-C from *A. paniculate*) were screened out to determine their inhibitory potentiality against M^{pro} and PL^{pro} by molecular docking analysis.

9. Conclusion

The current study is a screening-*based* study performed with the assistance of molecular docking and ADMET analysis tools/server and is now subject of matter to examine the activity of the compound potency of canthin-6-one 9-O-beta-glucopyranoside in inhibiting SARS-CoV-2 M^{pro}/$3CL^{pro}$ and PL^{pro}. The results of the MD simulation and binding free energy calculations indicated that canthin-6-one 9-O-beta-glucopyranoside compound interacted with the M^{pro} and PL^{pro} and can also be proposed as a potential natural drug molecule for the treatment of SARS CoV-2 (COVID 19).

10. Summary points

- SARS-CoV-2 is a beta coronavirus that spreads coronavirus disease 2019 (COVID-19) in the world leading to 74.29 million persons infected and 1.66 million death worldwide (222 countries, areas or territories with cases). The rapid spread of SARS-CoV-2 (COVID-19) has raised a severe global public health issue and creates a pandemic situation.
- The continuing SARS-CoV-2 pandemic makes us worryingly noticed that our present choices for nursing against deadly coronavirus disease are very restricted. Therefore, there is an instant need for the discovery of novel inhibitors attacking the vital viral proteins.
- The compounds of the three plants *viz. E. harmandiana, S. flavescens* and *A. paniculata* were screened for antiviral activity against the proteases of the 2019-nCov or SARS CoV-2.
- The molecular docking and ADMET analysis suggested that with less affinity and drug-likeness properties, canthin-6-one 9-O-beta-glucopyranoside is a potential molecule that binds to the M^{pro}/$3CL^{pro}$ and PL^{pro} and can inhibit the activity of replication and transcription of the virus and finally stop the multiplication of the virus. MD Simulation used to find best interaction and binding energy between

Fig. 4. (*continued*).

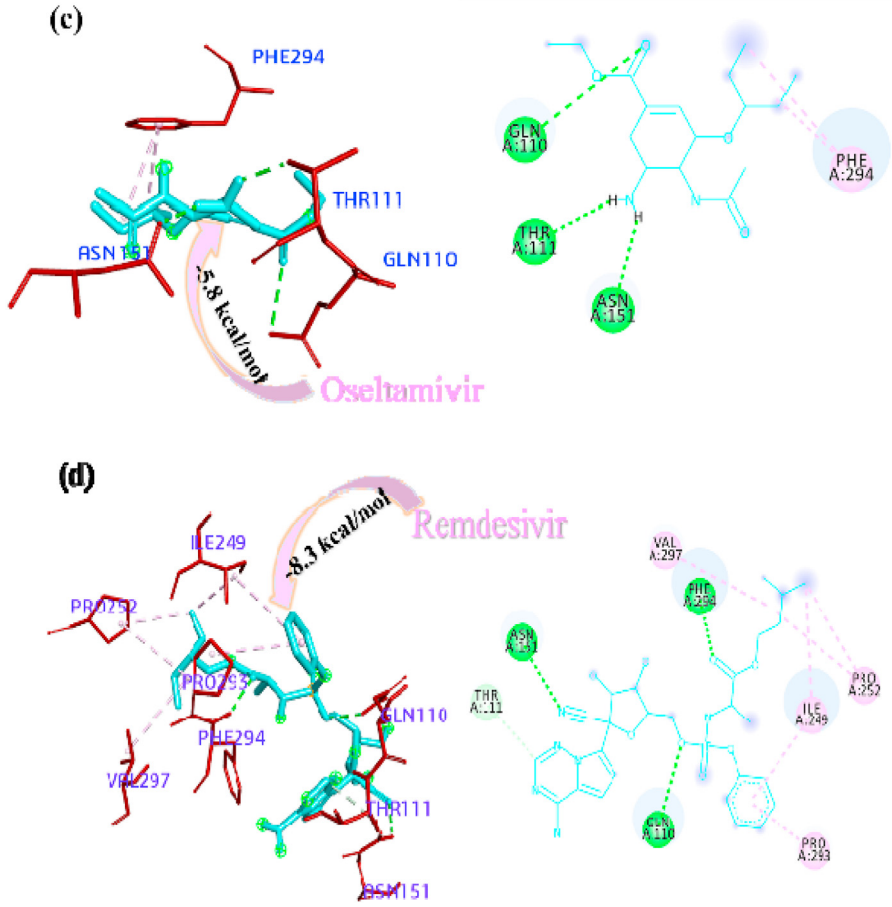

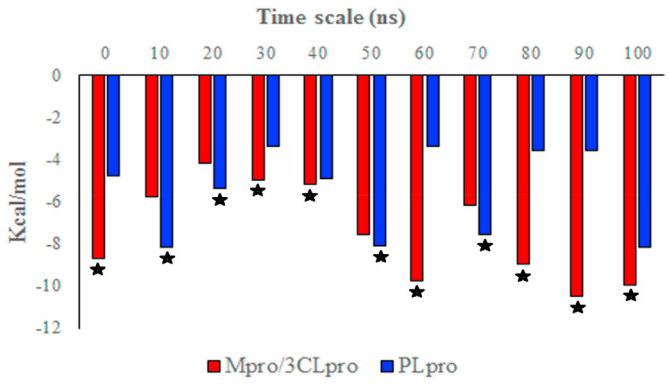

Fig. 5. Comparative binding energy of canthin-6-one 9-O-beta-glucopyranoside with M^{pro}/$3CL^{pro}$ and PL^{pro} (*energy values are the smaller in M^{pro}/$3CL^{pro}$ and PL^{pro} in respective time scale).

the canthin-6-one 9-O-beta-glucopyranoside and M^{pro}/$3CL^{pro}$ and PL^{pro} proteases of COVID19.

Author contributions

DM, MP and DV contributed equally as first authors. DV, DM, MP, PC, AK, DJ was involved in the writing; PKDM, HT, PJ, PP, RS, KP was involved in manuscript refinement & important intellectual content discussion; DV, AK was involved in molecular docking and DM initiated the idea of the study. MP carried out the MD simulation and related analyses along with binding energy calculation.

CRediT authorship contribution statement

Devvret Verma: Conception and design of study, Funding acquisition, Data curation, Formal analysis, Writing – original draft, and/or interpretation of data, Drafting the manuscript, Revising the manuscript critically for important intellectual content, Approval of the version of the manuscript to be published. **Debasis Mitra:** Conception and design of study, Funding acquisition, Data curation, Formal analysis, Writing – original draft, Acquisition of data, Analysis and/or interpretation of data, Drafting the manuscript, Revising the manuscript critically for important intellectual content, Approval of the version of the manuscript to be published. **Manish Paul:** Formal analysis, Data curation, Writing – original draft, Analysis and/or interpretation of data, Drafting the manuscript, Approval of the version of the manuscript to be published. **Priya Chaudhary:** Funding acquisition, Formal analysis, Data curation, Analysis and/or interpretation of data, Drafting the manuscript, Approval of the version of the manuscript to be published. **Anshul Kamboj:** Funding acquisition, Formal analysis, Data curation, Analysis and/or interpretation of data, Drafting the manuscript, Approval of the version of the manuscript to be published. **Hrudayanath Thatoi:** Revising the manuscript critically for important intellectual content, Approval of the version of the manuscript to be published. **Pracheta Janmeda:** Revising the manuscript critically for important intellectual content, Approval of the version of the manuscript to be published. **Divya Jain:** Approval of the version of the manuscript to be published. **Periyasamy Panneerselvam:** Revising the manuscript critically for important intellectual content, Approval of the version of the manuscript to be published. **Rakesh Shrivastav:** Revising the manuscript critically for important intellectual content, Approval of the version of the manuscript to be published. **Kumud Pant:** Revising the manuscript critically for important intellectual content, Approval of the version of the manuscript to be

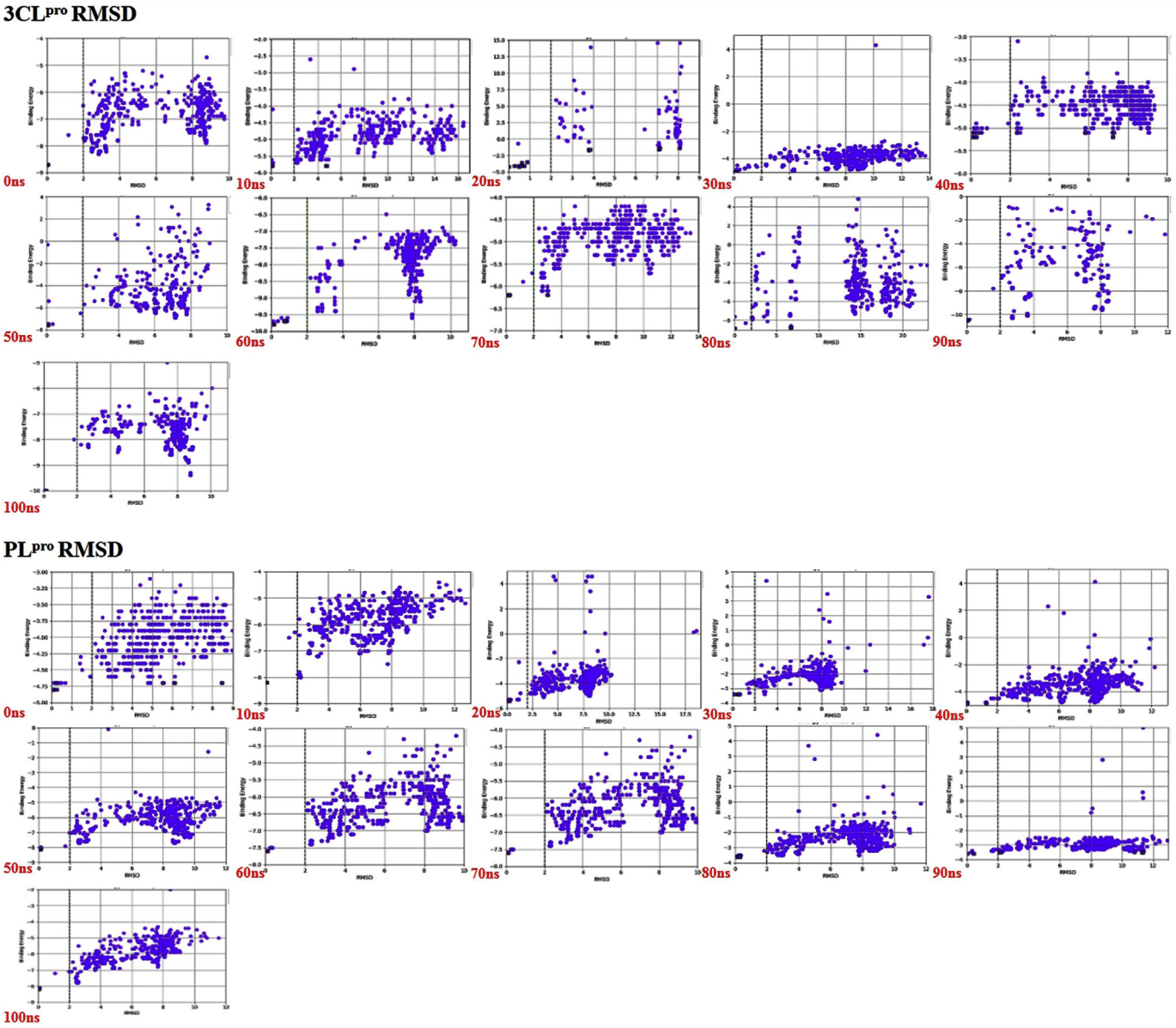

Fig. 6. Comparative RMSD vs. binding energy plots of canthin-6-One 9-O-beta-Glucopyranoside bound with M^{pro}/$3CL^{pro}$ and PL^{pro} calculated from MD simulation trajectory.

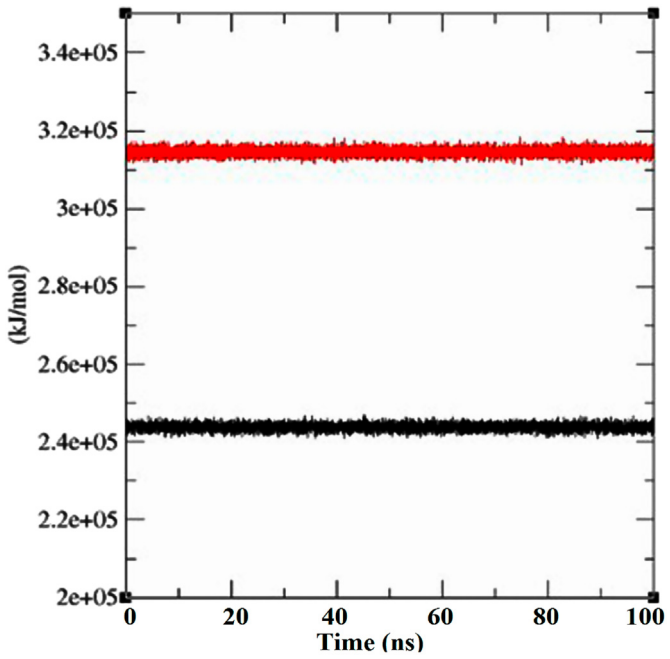

Fig. 7. Plot showing MM-PBSA calculation of canthin-6-One 9-O-beta-Glucopyranoside bound with M^{pro}/$3CL^{pro}$ (black) and PL^{pro} (red) calculated from MD simulation trajectory.

published. **Pradeep K. Das Mohapatra:** Revising the manuscript critically for important intellectual content, Approval of the version of the manuscript to be published.

Declaration of competing interest

The authors declare that there is no conflict of interest.

Acknowledgments

The authors are thankful to Graphic Era (Deemed to be University), Dehradun; Raiganj University, Raiganj; Maharaja Sriram Chandra Bhanja Deo University, Odisha; Banasthali Vidyapith, Vanasthali; ICAR- National Rice Research Institute, Cuttack; NGF College of Engineering and Technology, Palwal for the encouragement and support needed in the present investigation. Authors are grateful to the Bioinformatics Facility, Department of Biotechnology, Maharaja Sriram Chandra Bhanja Deo University, Baripada, India for the provision of computational support. The work was partially conducted in the context of the Bioinformatics Resources and Applications Facility (BRAF), C-DAC, Pune, India. D. Mitra is grateful to Government of West Bengal, India for Swami Vivekananda Merit Cum Means Ph.D. Scholarship (WBP191584588825). The authors are grateful to Dr. Isabella Zanella and Dr. Simon Pitchford, Guest Editor, Special Issue: COVID-19 therapy, from lung disease to systemic disorder, CRPHAR and reviewers for their valuable suggestions to increase the scientific quality of the manuscript.

Appendix A. Supplementary data

Supplementary data to this article can be found online at https://doi.org/10.1016/j.crphar.2021.100038.

Funding

n/a.

Intellectual property

We confirm that we have given due consideration to the protection of intellectual property associated with this work and that there are no impediments to publication, including the timing of publication, with respect to intellectual property. In so doing we confirm that we have followed the regulations of our institutions concerning intellectual property.

Research ethics

We further confirm that any aspect of the work covered in this manuscript that has involved human patients has been conducted with the ethical approval of all relevant bodies and that such approvals are acknowledged within the manuscript.

References

Aanouz, I., Belhassan, A., Ei-Khatabi, K., Lakhlifi, T., Ei-Idrissi, M., Bouachrine, M., 2020. Moroccan medicinal plants as inhibitors against SARS-CoV-2 main protease: computational investigation. J. Biomol. Struct. Dyn. https://doi.org/10.1080/07391102.2020.1758790.

Adeoye, A.O., Oso, B.J., Olaoye, I.F., Tijjani, H., Adebayo, A.I., 2020. Repurposing of chloroquine and some clinically approved antiviral drugs as effective therapeutics to prevent cellular entry and replication of coronavirus. J. Biomol. Struct. Dyn. https://doi.org/10.1080/07391102.2020.1765876.

Amin, S.A., Banerjee, S., Ghosh, K., Gayen, S., Jha, T., 2021. Protease targeted COVID-19 drug discovery and its challenges: insight into viral main protease (Mpro) and papain-like protease (PLpro) inhibitors. Bioorg. Med. Chem. 29, 115860. https://doi.org/10.1016/j.bmc.2020.115860.

Andres, F. Yepes-Pérez, Oscar, Herrera-Calderon, Quintero-Saumeth, Jorge, 2020. Uncaria tomentosa (cat's claw): a promising herbal medicine against SARS-CoV-2/ACE-2 junction and SARS-CoV-2 spike protein based on molecular modeling. J. Biomol. Struct. Dyn. https://doi.org/10.1080/07391102.2020.1837676.

Antunes, D.A., Moll, M., Devaurs, D., Jackson, K.R., Lizée, G., Kavraki, L.E., 2017. Dinc 2.0: a new protein–peptide docking webserver using an incremental approach. Canc. Res. 77 (21), e55–e57.

Arthur, D.E., Uzairu, A., 2019. Molecular docking studies on the interaction of NCI anticancer analogues with human Phosphatidylinositol 4, 5-bisphosphate 3-kinase catalytic subunit. J. King Saud Univ. Sci. 31, 1151–1166.

Arya, R., Das, A., Prashar, V., Kumar, M., 2020. Potential inhibitors against papain-like protease of novel coronavirus (SARS-CoV-2) from FDA approved drugs. ChemRxiv. https://doi.org/10.26434/chemrxiv.1186001.v2.

Astuti, I., Ysrafil, 2020. Severe Acute Respiratory Syndrome Coronavirus 2 (SARS-CoV-2): an overview of viral structure and host response. Diabetes metab Syndr 14 (4), 407–412. https://doi.org/10.1016/j.dsx.2020.04.020.

Barratt, E., Bingham, R.J., Warner, D.J., Laughton, C.A., Phillips, S.E., Homans, S.W., 2005. Van der Waals interactions dominate ligand– protein association in a protein binding site occluded from solvent water. J. Am. Chem. Soc. 127, 11827–11834.

Berman, H.M., Westbrook, J., Feng, Z., Gilliland, G., Bhat, T.N., Weissig, H., Shindyalov, I.N., Bourne, P.E., 2000. The protein data bank. Nucleic Acids Res. 28, 235–242.

Bharatiy, S.K., Hazra, M., Paul, M., Mohapatra, S., Samantaray, D., Dubey, R.C., Sanyal, S., Datta, S., Hazra, S., 2016. *In silico* designing of an industrially sustainable carbonic anhydrase using molecular dynamics simulation. ACS Omega 1 (6), 1081–1103.

Boopathi, S., Poma, A.B., Kolandaivel, P., 2020. Novel 2019 coronavirus structure, mechanism of action, antiviral drug promises and rule out against its treatment. J. Biomol. Struct. Dyn. 1–14.

Chaudhary, P., Janmeda, P., 2020. Spreadable virus of the 21st century: covid-19. Environ. Conserv. J. 21 (1&2), 13–18. https://doi.org/10.36953/ECJ.2020.211202.

Chen, C.P., Chen, C.C., Huang, C.W., Chang, Y.C., 2018. Evaluating molecular properties involved in transport of small molecules in stratum corneum: a quantitative structure-activity relationship for skin permeability. Molecules 23, 911.

Chowdhury, Papia, 2020. *In silico* investigation of phytoconstituents from Indian medicinal herb '*Tinospora cordifolia* (giloy)' against SARS-CoV-2 (COVID-19) by molecular dynamics approach. J. Biomol. Struct. Dyn. https://doi.org/10.1080/07391102.2020.1803968.

Daina, A., Michielin, O., Zoete, V., 2017. SwissADME: a free web tool to evaluate pharmacokinetics, drug-likeness and medicinal chemistry friendliness of small molecules. Sci. Rep. 7, 42717.

Dallakyan, S., Olson, A.J., 2015. Small-molecule library screening by docking with pyrx. Chem. Biol.: Methods Protocols.

Daneman, R., Prat, A., 2015. The blood–brain barrier. Cold Spring Harb. *Perspect. Biol.* 7, a020412.

Darden, T., Perera, L., Li, L., Pedersen, L., 1999. New tricks for modelers from the crystallography toolkit: the particle mesh Ewald algorithm and its use in nucleic acid simulations. Structure 7 (3), R55–R60.

Das, S., Sarmah, S., Lyndem, S., Roy, A.S., 2020. An investigation into the identification of potential inhibitors of SARS-CoV-2 main protease using molecular docking study. J. Biomol. Struct. Dyn. https://doi.org/10.1080/07391102.2020.1763201.

Dassault Systèmes Biovia, 2020. Discovery Studio, Release 2020. Dassault Systèmes, San Diego.
de Oliveira, O.V., Rocha, G.B., Paluch, A.S., Costa, L.T., 2020. Repurposing approved drugs as inhibitors of SARS-CoV-2 S-protein from molecular modeling and virtual screening. J. Biomol. Struct. Dyn. 1–14.
Elmezayen, Ammar D., Al-Obaidi, Anas, Şahin, Alp Tegin, Yelekçi, Kemal, 2020. Drug repurposing for coronavirus (COVID-19): *in silico* screening of known drugs against coronavirus 3CL hydrolase and protease enzymes. J. Biomol. Struct. Dyn. https://doi.org/10.1080/07391102.2020.1758791.
Enayatkhani, M., Hasaniazad, M., Faezi, S., Guklani, H., Davoodian, P., Ahmadi, N., Ali Einakian, M., Karmostaji, A., Ahmadi, K., 2020. Reverse vaccinology approach to design a novel multi-epitope vaccine candidate against COVID-19: an *in silico* study. J. Biomol. Struct. Dyn. 1–19. https://doi.org/10.1080/07391102.2020.1756411.
Enmozhi, S.K., Raja, K., Sebastine, I., Joseph, J., 2020. Andrographolide as a potential inhibitor of SARS-CoV-2 main protease: an *in-silico* approach. J. Biomol. Struct. Dyn. https://doi.org/10.1080/07391102.2020.1760136.
Ghosh, Rajesh, Chakraborty, Ayon, Biswas, Ashis, Chowdhuri, Snehasis, 2020. Evaluation of green tea polyphenols as novel corona virus (SARS CoV-2) main protease (Mpro) inhibitors – an in silico docking and molecular dynamics simulation study. J. Biomol. Struct. Dyn. https://doi.org/10.1080/07391102.2020.1779818.
Gyebi, Gideon A., Ogunro, Olalekan B., Adegunloye, Adegbenro P., Ogunyemi, Oludare M., Afolabi, Saheed O., 2020. Potential inhibitors of coronavirus 3-chymotrypsin-like protease (3CLpro): an *in silico* screening of alkaloids and terpenoids from African medicinal plants. J. Biomol. Struct. Dyn. https://doi.org/10.1080/07391102.2020.1764868.
Gyebi, G.A., Ogunro, O.B., Adegunloye, A.P., Ogunyemi, O.M., Afolabi, S.O., 2020. Potential inhibitors of coronavirus 3-chymotrypsin-like protease (3CLpro): an *in silico* screening of alkaloids and terpenoids from African medicinal plants. J. Biomol. Struct. Dyn. https://doi.org/10.1080/07391102.2020.1764868.
Han, Y., Zhang, X., Zhang, J., Hu, C.Q., 2019. *In silico* ADME and toxicity prediction of ceftazidime and its impurities. Front. Pharmacol. 10, 434.
Hasan, M.K., Kamruzzaman, M., Manjur, O.H.B., Mahmud, A., Hussain, N., Mondal, M.S.A., Hosen, M.I., Bello, M., Rahman, A., 2021. Structural analogues of existing anti-viral drugs inhibit SARS-CoV-2 RNA dependent RNA polymerase: a computational hierarchical investigation. Heliyon 7 (3), e06435.
Hess, B., Bekker, H., Berendsen, H.J., Fraaije, J.G., 1997. LINCS: a linear constraint solver for molecular simulations. J. Comput. Chem. 18 (12), 1463–1472.
JayaKumar, T., Hsieh, C.Y., Lee, J.J., Sheu, J.R., 2013. Experimental and clinical pharmacology of Andrographis paniculate and its major bioactive phytoconstituent Andrographolide. Evid. Based Complementary Altern. Med. 1–16. https://doi.org/10.1155/2013/846740.
Joshi, R.S., Jagdale, S.S., Bansode, S.B., Shankar, S.S., Tellis, M.B., Pandya, V.K., Chugh, A., Giri, A.P., Kulkarni, M.J., 2020. Discovery of potential multi-targeted-directed ligands by targeting host-specific SARS-CoV-2 structurally conserved main protease. J. Biomol. Struct. Dyn. https://doi.org/10.1080/07391102.2020.1760137.
Jyotisha, Samayaditya Singh, Ahmed Qureshi, Insaf, 2020. Multi-epitope vaccine against SARS-CoV-2 applying immunoinformatics and molecular dynamics simulation approaches. J. Biomol. Struct. Dyn. https://doi.org/10.1080/07391102.2020.1844060.
Kanchanapoom, T., Kasai, R., Chumsri, P., Hiraga, Y., Yamasaki, K., 2001. Canthin-6-one and β-carboline alkaloids from *Eurycoma harmandiana*. Phytochemistry 56, 383–386.
Khan, R.J., Jha, R.K., Amera, G.M., Jain, M., Singh, E., Pathak, A., Singh, R.P., Muthukumaran, J., Singh, A.K., 2020. Targeting SARS-CoV-2: a systematic drug repurposing approach to identify promising inhibitors against 3C-like proteinase and 2′-O-ribose methyltransferase. J. Biomol. Struct. Dyn. 1–14.
Kim, S., Thiessen, P.A., Bolton, E.E., Chen, J., Fu, G., Gindulyte, A., Han, L., He, J., He, S., Shoemaker, B.A., Wang, J., Yu, B., Zhang, J., Bryant, S.H., 2016. PubChem substance and compound databases. Nucleic Acids Res. 44, D1202–D1213.
Kim, J.H., Cho, I.S., So, Y.K., Kim, H.H., Kim Yh, Y.H., 2018. Kushenol A and 8-prenyl-kaempferol, tyrosinase inhibitors, derived from *Sophora flavescens*. J. Enzym. Inhib. Med. Chem. 33, 1048–1054. https://doi.org/10.1080/14756366.2018.1477776.
Konda, Mani Saravanan, Zhang, Haiping, Renganathan, Senthil, Kumar Vijayakumar, Kevin, Sounderrajan, Vignesh, Wei, Yanjie, Shakila, Harshavardhan, 2020. Structural basis for the inhibition of SARS-CoV2 main protease by Indian medicinal plant-derived antiviral compounds. J. Biomol. Struct. Dyn. https://doi.org/10.1080/07391102.2020.1834457.
Kumar, Y., Singh, H., 2020. *In Silico* Identification and Docking-Based Drug Repurposing against the Main Protease of SARS-CoV-2, Causative Agent of COVID-19. ChemRxiv.
Kumar, D., Kumari, K., Jayaraj, A., Kumar, V., Kumar, R.V., Dass, S.K., Chandra, R., Singh, P., 2020a. Understanding the binding affinity of noscapines with protease of SARS-CoV-2 for COVID-19 using MD simulations at different temperatures. J. Biomol. Struct. Dyn. 1–14. https://doi.org/10.1080/07391102.2020.1752310.
Kumar, V., Dhanjal, J.K., Kaul, S.C., Wadhwa, R., Sundar, D., 2020b. Withanone and Caffeic acid Phenethyl ester are predicted to Interact with main protease (Mpro) of SARS-CoV-2 and inhibit its activity. J. Biomol. Struct. Dyn. 1–17.
Kumari, R., Kumar, R., 2014. Open source drug discovery Consortium, & Lynn A. g_mmpbsa- A GROMACS tool for high-throughput MM-PBSA calculations. J. Chem. Inf. Model. 54 (7), 1951–1962.
Li, D., Luan, J., Zhang, L., 2021. Molecular docking of potential SARS-CoV-2 papain-like protease inhibitors. Biochem. Biophys. Res. Commun. 538, 72–79. https://doi.org/10.1016/j.bbrc.2020.11.083.
Lin, L.-T., Hsu, W.-C., Lin, C.-C., 2014. Antiviral natural products and herbal medicines. J Tradit Complement Med 4 (1), 24–35. https://doi.org/10.4103/2225-4110.124335.
Lobo-Galo, N., Terrazas-López, M., Martínez-Martínez, A., Díaz-Sánchez, A.G., 2020. FDA-approved thiol-reacting drugs that potentially bind into the SARS-CoV-2 main protease, essential for viral replication. J. Biomol. Struct. Dyn. 1–12.
Maroli, Nikhil, Bhasuran, Balu, Natarajan, Jeyakumar, Kolandaivel, Ponmalai, 2020. The potential role of procyanidin as a therapeutic agent against SARS-CoV-2: a text mining, molecular docking and molecular dynamics simulation approach. J. Biomol. Struct. Dyn. https://doi.org/10.1080/07391102.2020.1823887.
McKee, D.L., Sternberg, A., Stange, U., Laufer, S., Naujokat, C., 2020. Candidate drugs against SARS-CoV-2 and COVID-19. Pharmacol. Res. 157, 104859. https://doi.org/10.1016/j.phrs.2020.104859.
Meng, X.Y., Zhang, H.X., Mezei, M., Cui, M., 2011. Molecular docking: a powerful approach for structure-based drug discovery. Curr Comput-Aid Drug 7, 146–157.
Mitjà, O., Clotet, B., 2020. Use of antiviral drugs to reduce COVID-19 transmission. Lancet Glob Health 8, e639–e640.
Mitra, D., Verma, D., Mahakur, B., Kamboj, A., Srivastava, R., Gupta, S., Pandey, A., Arora, B., Pant, K., Panneerselvam, P., Ghosh, A., Barik, D., Das Mohapatra, P.K., 2021. Molecular docking and simulation studies of natural compounds of *Vitex negundo* L. against papain-like protease (PLpro) of SARS CoV-2 (coronavirus) to conquer the pandemic situation in the world. J. Biomol. Struct. Dyn. 39, 1–22. https://doi.org/10.1080/07391102.2021.1873185.
Miyamoto, S., Kollman, P.A., 1992. Molecular dynamics studies of calixspherand complexes with alkali metal cations: calculation of the absolute and relative free energies of binding of cations to a calixspherand. J. Am. Chem. Soc. 114 (10), 3668–3674.
Mohamed, A.H., Fatima, A.J., 2020. Covid-19 induced superimposed bacterial infection. J. Biomol. Struct. Dyn. 1–18. https://doi.org/10.1080/07391102.2020.1772110.
Mukhtar, M., Arshad, M., Ahmad, M., Pomerantz, R.J., Wigdahl, B., Parveen, Z., 2008. Antiviral potentials of medicinal plants. Virus Res. 131 (2), 111–120.
Muralidharan, N., Sakthivel, R., Velmurugan, D., Gromiha, M.M., 2020. Computational studies of drug repurposing and synergism of lopinavir, oseltamivir and ritonavir binding with SARS-CoV-2 Protease against COVID-19. J. Biomol. Struct. Dyn. 1–6.
Mussard, E., Cesaro, A., Lespessailles, E., Legrain, B., Berteina-Raboin, S., Toumi, H., 2019. Andrographolide, a natural antioxidant: an update. Antioxidants 8, 571. https://doi.org/10.3390/qntiox8120571.
Pajouhesh, H., Lenz, G.R., 2005. Medicinal chemical properties of successful central nervous system drugs. NeuroRx 2, 541–553.
Páll, S., Abraham, M.J., Kutzner, C., Hess, B., Lindahl, E., 2015. Tackling exascale software challenges in molecular dynamics simulations with GROMACS. In: International Conference on Exascale Applications and Software. Springer, Cham, pp. 3–27.
Pirzada, R.H., Haseeb, M., Batool, M., Kim, M., Choi, S., 2021. Remdesivir and Ledipasvir among the FDA-approved antiviral drugs have potential to inhibit SARS-CoV-2 replication. Cells 10 (5), 1052.
Priya, Shree, Mishra, Priyanka, Selvaraj, Chandrabose, Singh, Sanjeev Kumar, Chaube, Radha, Garg, Neha, Tripathi, Yamini Bhusan, 2020. Targeting COVID-19 (SARS-CoV-2) main protease through active phytochemicals of ayurvedic medicinal plants – *Withania somnifera* (Ashwagandha), *Tinospora cordifolia* (Giloy) and *Ocimum sanctum* (Tulsi) – a molecular docking study. J. Biomol. Struct. Dyn. https://doi.org/10.1080/07391102.2020.1810778.
Rafi, M., Devi, A.F., Syafitri, U.D., Heryanto, R., Suparto, I.H., Amran, M.B., Rohman, A., Prajogo, B., Lim, L.W., 2020. Classification of *Andrographis paniculate* extracts by solvent extraction using HPLC fingerprint and chemometric analysis. BMC Res. Notes 13, 56. https://doi.org/10.1186/s13104-020-4920-x.
Razzaghi-Asl, Nima, Ahmad, Ebadi, Shahabipour, Sara, Gholamin, Danial, 2020. Identification of a potential SARS-CoV2 inhibitor via molecular dynamics simulations and amino acid decomposition analysis. J. Biomol. Struct. Dyn. https://doi.org/10.1080/07391102.2020.1797536.
Ribaudo, Giovanni, Alberto, Ongaro, Oselladore, Erika, Zagotto, Giuseppe, Memo, Maurizio, Gianoncelli, Alessandra, 2020. A computational approach to drug repurposing against SARS-CoV-2 RNA dependent RNA polymerase (RdRp). J. Biomol. Struct. Dyn. https://doi.org/10.1080/07391102.2020.1822209.
Rolta, Rajan, Yadav, Rohitash, Salaria, Deeksha, Trivedi, Shubham, Imran, Mohammad, Sourirajan, Anuradha, Baumler, David J., Dev, Kamal, 2020. *In silico* screening of hundred phytocompounds of ten medicinal plants as potential inhibitors of nucleocapsid phosphoprotein of COVID-19: an approach to prevent virus assembly. J. Biomol. Struct. Dyn. https://doi.org/10.1080/07391102.2020.1804457.
Salim, B., Noureddine, M., 2020. Identification of compounds from Nigella sativa as new potential inhibitors of 2019 novel coronaviruses (covid-19): molecular docking study. ChemRxiv. https://doi.org/10.20944/preprints202004.0079.v1.
Schüttelkopf, A.W., van Aalten, D.M.F., 2004. PRODRG: a tool for high-throughput crystallography of protein-ligand complexes. Acta Crystallogr. D60, 1355–1363.
Selvaraj, Alagu Lakshmi, Raja Mohamed, Beema Shafreen, Arumugam, Priya, Karutha Pandian, Shunmugiah, 2020. Ethnomedicines of Indian origin for combating COVID-19 infection by hampering the viral replication: using structure-based drug discovery approach. J. Biomol. Struct. Dyn. https://doi.org/10.1080/07391102.2020.1778537.
Shahbaaz, Mohd, Amir, Mohd, Rahman, Safikur, Mustafa Hasan, Gulam, Dohare, Ravins, Krishna, Bisetty, Ahmad, Faizan, Kim, Jihoe, Hassan, Md Imtaiyaz, 2018. Structural insights into Rab21 GTPase activation mechanism by molecular dynamics simulations. Mol. Simulat. 44 (3), 179–189.
Sharma, A., Tiwari, S., Deb, M.K., Marty, J.L., 2020. Severe acute respiratory syndrome coronavirus-2 (SARS-CoV-2): a global pandemic and treatment strategies. Int. J. Antimicrob. Agents 10, 106054. https://doi.org/10.1016/j.ijantimicagh.2020.106054.

Subhomoi, B., Banerjee, M., 2020. A computational prediction of SARS-CoV-2 structural protein inhibitors from *Azadirachta indica* (Neem). J. Biomol. Struct. Dyn. https://doi.org/10.1080/07391102.2020.1774419.

Suyash, Pant, Singh, Meenakshi, Ravichandiran, V., Murty, U.S.N., Srivastava, Hemant Kumar, 2020. Peptide-like and small-molecule inhibitors against Covid-19. J. Biomol. Struct. Dyn. https://doi.org/10.1080/07391102.2020.1757510.

Tallei, T., Tumilaar, S.G., Niode, N., Fatimawali, F., Kepel, B., Idroes, R., Effendi, Y., 2020. Potential of Plant Bioactive Compounds as SARS-CoV-2 Main Protease (Mpro) and Spike (S) Glycoprotein Inhibitors: a Molecular Docking Study. https://doi.org/10.20944/preprints202004.0102.v2.

The PyMOL Molecular Graphics System, 2020. Version 1.2r3pre. Schrödinger, LLC. https://pymol.org/2/.

Fatoki, Toluwase Hezekiah, Ibraheem, Omodele, Ogunyemi, Ibukun Oladejo, Akinmoladun, Afolabi Clement, Ugboko, Harriet U., Adeseko, Catherine Joke, Awofisayo, Oladoja A., Olusegun, Sunday Joseph, Enibukun, Jesupemi Mercy, 2020. Network analysis, sequence and structure dynamics of key proteins of coronavirus and human host, and molecular docking of selected phytochemicals of nine medicinal plants. J. Biomol. Struct. Dyn. https://doi.org/10.1080/07391102.2020.1794971.

Trott, O., Olson, A.J., 2010. AutoDock Vina: improving the speed and accuracy of docking with a new scoring function, efficient optimization, and multithreading. J. Comput. Chem. 31, 455–461. https://doi.org/10.1002/jcc.21334.

ul Qamar, M.T., Maryam, A., Muneer, I., Xing, F., Ashfaq, U.A., Khan, F.A., Anwar, F., Geesi, M.H., Khalid, R.R., Rauf, S.A., Siddiqi, A.R., 2019. Computational screening of medicinal plants phytochemicals to discover potent pan-seotype inhibitors against dengue virus. Sci. Rep. 9, 1433. https://doi.org/10.1038/s41598-018-38450-1.

V'kovski, P., Kratzel, A., Steiner, S., Stalder, H., Thiel, V., 2020. Coronavirus biology and replication: implications for SARS-CoV-2. Nat. Rev. Microbiol. 19, 155–170. https://doi.org/10.1038/s41579-020-00468-6.

van Gunsteren, W.F., Billeter, S.R., Eising, A.A., Hünenberger, P.H., Krüger, P.K.H.C., Mark, A.E., Tironi, I.G., 1996. Biomolecular Simulation: the GROMOS96 Manual and User Guide. Vdf Hochschulverlag AG an der ETH Zürich, Zürich, p. 86.

Vaught, A., 1996. Graphing with Gnuplot and Xmgr: two graphing packages available under linux. Linux J. 1996 (28es), 7.

Vimal, K. Maurya, Kumar, Swatantra, Madan, L., Bhatt, B., Saxena, Shailendra K., 2020. Antiviral activity of traditional medicinal plants from Ayurveda against SARS-CoV-2 infection. J. Biomol. Struct. Dyn. https://doi.org/10.1080/07391102.2020.1832577.

Weber, W., Hünenberger, P.H., McCammon, J.A., 2000. Molecular dynamics simulations of a polyalanine octapeptide under Ewald boundary conditions: influence of artificial periodicity on peptide conformation. J. Phys. Chem. B 104 (15), 3668–3675.

World Health Organization, 2020. Coronavirus disease (COVID-19): situation report-107. https://www.who.int.

Wu, R., Wang, L., Dina Kuo, H.C., Shannar, A., Peter, R., Chou, P.J., Li, S., Hudlikar, R., Liu, X., Liu, Z., Poiani, G.J., Amorosa, L., Brunetti, L., Kong, A.N., 2020. An update on current therapeutic drugs treating COVID-19. Curr. Pharmacol. Rep. 11, 1–15. https://doi.org/10.1007/s40495-020-00216-7.

Zainib, Babar, Khan, Mazhar, Zahra, Mubeen, Anwar, Munazza, Noor, Kashif, Hashmi, Huma Farooque, Suleman, Muhammad, Waseem, Muhammad, Shah, Abdullah, Ali, Shahid, Ali, Syed Shujait, 2020. Drug similarity and structure-based screening of medicinal compounds to target macrodomain-I from SARS-CoV-2 to rescue the host immune system: a molecular dynamics study. J. Biomol. Struct. Dyn. https://doi.org/10.1080/07391102.2020.1815583.

Zhang, L., Shen, F.M., Chen, F., Lin, Z., 2020a. Origin and evolution of the 2019 novel coronavirus. Clin. Infect. Dis. https://doi.org/10.1093/cid/ciaa112.

Zhang, H., Penninger, J., Li, Y., Zhong, N., Slutsky, A.S., 2020b. Angiotensin-converting enzyme 2 (ACE2) as a SARS-CoV-2 receptor: molecular mechanisms and potential therapeutic target. Intensive Care Med. 46, 586–590. https://doi.org/10.1007/s00134-020-05985-9.